

We would like to thank the reviewer for the constructive comments and the helpful suggestions to improve this manuscript, especially in the context of trying to use this work to inform future research in the area, as this aligns very well with our future goals. In the following the reviewer comments are shown in blue, and our responses in black.

1. Where does the gas-phase chemistry leave and the VBS take over? Page 2 highlights how auto-oxidation is similar to other RO₂ fates (+NO or +HO₂) whose products can be treated by a VBS. The RO₂+HO₂, etc is not predicted by the VBS, but a gasphase mechanism. Would it be more accurate (e.g. to state in the abstract) that “a new implementation of the VBS that explicitly resolves peroxy radical (RO₂) PRODUCTS formed via auto-oxidation”? When do the kernels take over? At a specific volatility? Would a chemical transport model use the VBS (or kernels) to predict auto-oxidation?

We added the suggested language to the abstract to clarify that yes, a gas-phase mechanism predicts the reaction yields and the volatility yields are resolved using kernels following that. In this framework the RO₂ radicals are always treated within the chemical mechanism and their molecular products resolve into the VBS (so auto-oxidation is treated within the mechanism). The attribute for any RO₂ in the chemical mechanism, including within a CTM, to be resolved into the VBS is a volatility (C°) estimate and O:C. In this implementation all RO₂ are resolved into the VBS but this is in part because we are only modeling α -pinene oxidation and even the initial RO₂ has a relatively low (SVOC) C° ; implementations for a richer chemistry will be free to select any subset of all RO₂ to resolve into a VBS and also to lump RO₂ were that desired.

2. The work is highly idealized and hypothetical and could be informed by recent mechanistic work on the α -pinene system. Future work (aimed at, for example, estimating auto-oxidation rate constants and RO₂+RO₂ dimer rates) could also be better informed if some of the already published parameters were considered in this work.

We chose not to directly simulate individual experiments because we are reluctant to attach meaning to the tuned parameters that would result in such an exercise. Further, it would require a well-vetted model of each experiment, which would in our opinion obscure the message of this paper. This is based on past experience. As an example, equilibrium interpretation of chamber experiments, extending from Odum et al., through many of our own VBS analyses of chamber experiments, was ultimately found to be erroneous for two reasons. First, the dynamics of SOA condensation is often important, and, second, vapor losses to chamber walls can vary between experiments and within experiments in ways that make mass yields appear low at low overall aerosol mass (really Fuchs-adjusted surface area) loadings. The only parameters in the equilibrium model capable of reproducing the rising mass yields with rising loadings were the VBS bin mass yields themselves. The resulting fits were not only good but they were highly predictive (including temperature effects) in part because they implicitly contained chamber effects and these effects reasonably transferred from one experiment to another. However, the entire tongue of (UE)LVOCs that are the major topic of this paper was completely missing from those fits, and the inference was an SOA population that was far more “semi volatile” than now appears to be appropriate. This was compounded by the lack of a chemical mechanism to explain that low-volatility tongue (without auto oxidation, HOMs, and dimers). The more semi-volatile SOA was far more consistent with the then canonical oxidation mechanisms, making the whole scheme self consistent but, ultimately, incomplete in important ways.

Rather than directly comparing to experiments, our approach is to use the (often uncertain and sometimes contradictory) current experimental findings as constraints on the kinetic parameters of our model current simple model. There are at least two areas where our simple scheme may well ultimately require more nuance before more direct comparisons with experiments is fruitful. Both are related to the diversity of chemical behavior likely in the (many) peroxy radicals arising even from a single precursor such as α -pinene. Fortunately, the rate coefficients and products for reactions with NO and HO₂ appear to be relatively constant across a sequence of RO₂ radicals, but the RO₂ cross reactions and also the auto-oxidation rate constants are highly variable. Rather than a single tongue of progressively more oxidized RO₂, which we currently employ, it is likely that we will require at least a “less reactive” and “more reactive” RO₂ at each stage of auto-oxidation. It is unclear whether “less” and “more” will apply equally to the internal H-atom transfers and the RO₂ cross reactions, so even more diversity may be in order.

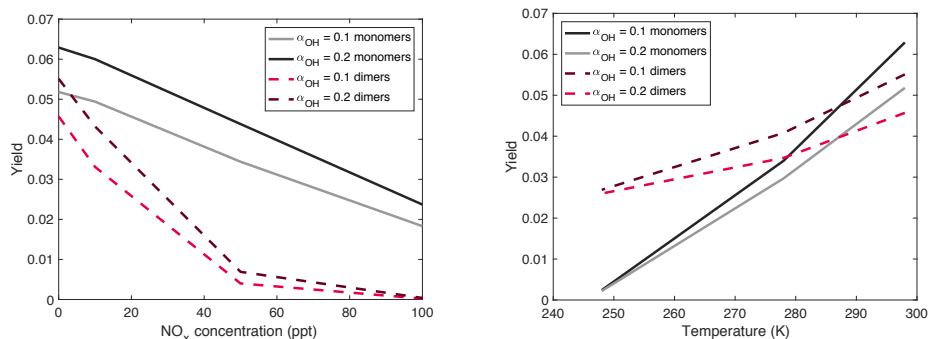
It is unlikely that aggregate fits and comparisons with bulk measures such as SOA mass and nucleation rates will be useful constraints for these RO₂ kinetics parameters. Rather, the emerging set of kinetics data on individual reactions will need to be used to define the mechanism itself; however, in our opinion the phase space of RO₂ reactions is too large to make that fruitful right now.

a. The authors assert OH radical-derived RO₂ do no auto-oxidize as readily as ozone initiated ones with a reference to Ehn et al. 2014 (page 4). Berndt et al. 2016 found that quantification of the OH-initiated HOMs from α -pinene are highly sensitive to the detection technique and that previous work likely underestimated them. Revise in consideration of this more recent work.

This is a valid point but there are other constraints as well. For example, Kirkby et al. (2016) found that the nucleation rate associated with additional oxidation of α -pinene by OH (after initial ozonolysis, as simulated here) had only a small effect on the observed new-particle formation rates. This is consistent with OH oxidation having lower overall HOM yields than ozonolysis (and inconsistent with similar yields). However, the point is well taken that it is appropriate to consider a range of the HOM yields from OH oxidation, and so we will revise the manuscript to consider a higher HOM yield from OH in addition to our base-case lower yield. This does not change our conclusions about the temperature and NO dependence of the processes.

b. Rather than specifying one value per oxidant for the fraction of RO₂ able to undergo auto-oxidation (alpha, page 6), can the authors provide insight into a plausible range? For example, the alpha for OH is set at 0.1 while Vereecken et al., 2007, Berndt et al., 2016, and Pye et al., 2019 all suggest values on the order of 0.2. Can one of those values (0.1 or 0.2) be ruled out or are they both plausible?

An α value of 0.2 is completely reasonable within this framework. We do not present a full sensitivity analysis but instead hold some parameters constant, such as α . However, we have explored the sensitivity parameters including α , the RO₂ isomerization barrier height and pre-factor, the dimer formation rate constant, etc. What we find is a substantial co-variance among these parameters suggesting a complex parameter phase space with many possible parameter sets producing equally “good” results. Again, because our objective in this work is to explore the sensitivity of the HOM yields to temperature and NO, more than to describe their absolute yields, we chose to hold this parameter fixed for the sake of simplicity. The effect of these two parameters on the temperature and NO_x dependencies are relatively small, as can be seen in the figure at the end of the response.



c. You may want to consider examining faster auto-oxidation rate constants (3-10 1/s) and add a-pinene RO₂+RO₂ specific values (Section 3.1.3-3.1.5) based on literature (Zhao et al. 2019).

We do address this by allowing the isomerization pre-factor to vary, as shown in Figure 9. Qualitatively, the high-temperature HOM (monomer + dimer) yields increase to essentially all of the HOMs allowed by the parameter α , and only drop once it is cold enough to slow down the isomerization enough for bimolecular reactions to compete. Likewise, it requires proportionally more NO to quench the RO₂. As we discussed above, it is possible that to adequately describe auto-oxidation, its effects on new-particle formation as well as SOA formation, and the sensitivity of both to NO, T, HO₂, etc, we will need to treat “fast” and “slow” reacting RO₂. There is ample evidence in the kinetic literature for a high degree of variability in both the RO₂ cross reactions and the auto-oxidation rate. Equally, we are unsure whether the RO₂ species are directly comparable in the relatively low-concentration, long timescale experiments such as CLOUD and the relatively high-concentration, short timescale experiments such as flowtubes.

We will add text in a revised manuscript to make this clearer.

d. How does the value of gamma (page 8) predicted in this work match up with gamma from mechanistic work (e.g. Zhao et al. 2019)?

The γ value ranges from 10^{-8} for the least oxidized RO₂s to 0.9 for the most oxidized at 298 K. The value of gamma is dependent on the C_{ref}^o , which is dependent on temperature, but these values are the lowest for each peroxy radical over the temperature range investigated here. Zhao et al. predict a minimum gamma value of 0.04. For most of the association reactions, our γ values agree with their work. However, their work also predicts slower rate constants than used here, which had we used, we would need higher gamma values.

e. Why wasn't an actual a-pinene experiment simulated? How well would the parameterization perform?

As discussed above, we did not simulate individual experiments because the large number of tunable parameters would allow us to reproduce a data set fairly easily without providing more clarity on the parameters. For example making the auto-oxidation rate constant faster would cause more oxidized products to be form and keeping everything else the same would lead to more HOM formation. But if we simultaneously slow down the dimerization rate constants and the unimolecular rate constant, we may be able to return to the same picture we present in this paper with a different set of parameters. We would also need to develop a corresponding chamber or flow-tube model, with appropriate wall-loss treatment, to properly model any individual experiment. The uncertain parameters associated with that reactor model would further confound the analysis.

f. Page 12, line 33: “NOx suppresses dimer yields more aggressively than it does HOM monomer yields.? How likely is this to be generally applicable to the atmosphere? Can you modify rate constants and branching to state with more/less confidence what the NOx modulation of HOM is?”

Lehtipalo et al., 2018 reported strong decreases in dimer yields coupled with an increase in total HOM yields due to nitrate-containing monomers in chamber experiments. However, this is another case where the full potential array of parameters leaves several possibilities open. One possibility is that the isomerization rate coefficient important here remain relatively constant as the auto-oxidation progresses (this is our base case). Another is that the initial isomerization rate coefficient is relatively slow and these accelerate with increasing functionalization. In that case the initial RO₂ would be a significant bottleneck and NO could

substantially quench both HOM monomer and dimer formation.

g. Page 13, line 23: what bounds do you propose for the auto-oxidation rate coefficient? The bounds on the carbon yield in Fig 9 can be quite large (the min/max bound is also hard to see and link with monomer vs dimer).

We allow the rate coefficient to vary through two parameters – the barrier and the A factor (Fig 8 and Fig 9). We suggest bounds of $7500 < E_a < 9000$ K or approximately 15-18 kcal/mol for the barrier (with the rate constant fixed at 300) and $(10, 7, 6) \times 10^{7 \pm 1}$. This low end range allows auto-oxidation to be competitive with fast bimolecular reactions

and to have the strong temperature dependence that is seen experimentally. The high end of this range is when the barrier becomes too high to overcome even at high temperatures where we expect to see a significant fraction of auto-oxidized products.

3. How generalizable are the parameters within the a-pinene system and to other systems? Previous work (e.g., Kurten et al., 2017) has highlighted how structure specific product distributions can be. Can the a-pinene system be treated with a series of general kernels or will we eventually need an explicit mechanism that replaces the specified values of alpha, the dimer kernel, etc. with individual species and unique yields? How important is it to capture the diversity of barriers and rate constants (page 6)? Can you provide some bounds for what might be good enough?

It is important to capture the diversity of of barriers and rate constants, however being able to group peroxy radicals as we did here would allow for a much simpler implementation into chemical models. Without specific rate constants for every peroxy radical being produced, here we seek to group the peroxy radicals by the extent of oxidation they have undergone. There is evidence in Kurten et al and Zhao et al 2019 that these trends may be present, however in the future comparison with a more explicit chemical mechanism would be able to tell us what is “good enough.”

1. Page 2, line 9-add units after 300

Done.

2. Page 2, clarify Co is volatility at temperature, T?

We plot everything using $C^*(300)$ as the x-axis so as to visualize how the products of the chemistry are changing rather and inferring how this would affect condensation. This language was added on page 2.

3. Page 6, section 3.1.2: what are the parameters (A) based on?

The value of A was chosen to give auto-oxidation rate constants of about 0.01 s^{-1} while maintaining a high barrier for a strong temperature dependence.

4. Section 3.1.3 and 3.1.5 both cover RO2 cross reactions. How are they connected?

They are the same reaction, however not all association reactions form dimers as some may form 2 alkoxy radicals that stabilize with other radicals to form monomers. Section 3.1.3 and 3.1.4 were switched as 3.1.3 and 3.1.5 are in fact very closely related.

5. Page 9, line 9-add units after 300. Note additional appearances of 300 should be 300 K throughout the manuscript.

This was fixed.

6. Page 11, near line 20, Does the LVOC characterization apply based on the C^* at Tref or C^* at T? Is the definition of LVOC, ELVOC, etc environment dependent or unique to the species? Also page 11, line 32 ? . . .the volatility classes shift toward higher Co (300) at lower temperature. . . ? is a bit confusing.

The LVOC range is different at every temperature. It is visually represented in Figs 5 and 6, but we agree the written language is confusing and page 11 line 20 has been restated.

We would like to thank the reviewer for the constructive comments and for bringing to our attention some clarity issues that we have attempted to address. In the following the reviewer comments are shown in blue, and our responses in black.

Page 8, line 17. “here we shall explore the possibility that. . .” I was expecting more exploration, for example with different scenarios. Instead it seems like just one situation was considered.

The efficiency of dimer formation is in our assessment a rapidly moving target. Other than the empirical observation that very highly oxidized RO₂ appear to make dimers with high efficiency and very small RO₂ (i.e. CH₃O₂) appear to make little or no dimer, the territory in the middle is uncertain. The efficiency of the avoid curve crossing may well scale with some combination of the oxygenated functional groups near the ROO moieties as well as cluster stabilization allowing for a longer interaction time (functionally the same phenomenon we are exploring here). For this reason we kept a single mechanism for dimer formation in this work; however, it is important to note that this causes the dimer production in our model to extend to ever less functionalized, less oxidized RO₂ as temperature decreases. Temperature dependent measurements of dimer yields with instruments sensitive to the full range of dimers would provide an excellent constraint here.

Page 8 line 26. Is the value of C^o(ref) ever defined? Were different values considered (explore!)?

The value of C^o(ref) used in this work is 10⁻² at 298 K and moves 1 order of magnitude lower in volatility per 10 K reduction in temperature. We explored different values of C^o(ref) during model development; however, we chose to hold it constant at each temperature for the results presented here to limit the number of tunable parameters in the simulation.

Page 9 line 3. Here (and in a few other places) a-pinene “oxidation” is referred to. Maybe be a little more clear by specifying “ozonolysis”.

We use the word “oxidation” to add generality as α-pinene may be oxidized by ozone, OH, or NO₃ when NO_x is present. Our simulations are thus driven initially by ozonolysis but include all three oxidants.

Page 11, line 5. I don’t see the factor of 40-80 in the figure. Looks more like 10 or 20.

The RO₂ in Fig. 4 are the “OxRO₂” including at least one -OOH group as shown also in Fig. 3. As one can see in Fig. 2, the “simple” RO₂ also has a maximum concentration above 2.5 × 10⁸ cm⁻³ so the sum is well over 2.5 × 10⁸. We have clarified this in the figures and text.

Page 11, line 6. Is this the first reference to photolysis being “on”? Maybe it should be mentioned in the general description of the set up on Page 10. Until then, I had assumed the ozonolysis would take place in the dark.

In the revised manuscript we make it clear at the onset that photochemistry is involved.

Figure 4 could maybe be made a little clearer. It took me a while, but I eventually figured out that the labels on the right axis corresponded to the HO2 and RO2 for the different NO_x levels.

The top legend incorrectly labeled the blue curves as “NO_x”; they are “NO” and we have corrected this. We have also added to the caption to emphasize that the labels along the right-hand y-axis refer to the NO_x concentration for each simulation by inserting “The numbers along the right-hand y-axis refer to the NO_x concentration for each simulation, which is also indicated by the shading of each curve, going from light at low NO_x to dark at high NO_x”.

Supplemental Table, page 2. The branching from AP + O₃ seems to contradict the text. Here, the radical RO₂ is allowed to isomerize, so it actually corresponds to OxoRO₂ in the text. So the yield should be 0.25 not 0.75? The less reactive radical SVOC should then correspond to RO₂ in the text.

Kudos and thank you for close reading! This was a typo in the supplemental material, which we corrected. The main text is correct.

Do the SVOC/RO₂ radicals participate in subsequent chemistry (reaction with HO₂, cross reactions)?

Yes, the peroxy radicals that we do not allow to isomerize may still participate in any of the termination chemistry.

Also, the coefficients in the Table are all 0.75/0.25, while in the text it is stated that alpha(OH) is 0.1 and alpha(NO₃) is 0. Just typos? This all needs to be tidied up.

Once again, thank you. These were typos in the supplemental table; the main text is correct and we corrected the typos.

Page 1, line 21. “are” is repeated.

Fixed.

Page 12, line 23. “at” should be “a”.

Yep.

Figure 2. Left axis should read “concentration”. Caption line 2. Is a little simplistic. Of course the radicals are reacting away all the time. It’s just that the source (a-pinene + O₃) is reduced)

The revised caption reads “as α-pinene decays and the RO₂ react away”

Figure 4, caption. “before gradually decaying”. Does this refer to their behavior with time, or as a function of NO?

We added “As a function of time” to the end of the caption to make this clear.

Figure 5. This is probably a stylistic thing. I find the lengthy caption inappropriate. Much of this is discussion, which might be better off in the text. I prefer captions to be punchy, with just enough description to be able to understand the figure (which isn’t always the case here).

We simplified the caption and moved some discussion to the main text while retaining enough substance so that a casual reader can understand the figure while scanning over just the “storyboard” of figures, which is our objective. We also reworked the caption so that the sense is temperature increasing; this allows the reader to more easily scan the figures in the natural direction from left to right.

Figure 6, caption. Delete “without”.

Done.

Figures in general. A couple of times, the top of a curve is missing (figs 3 and 8, for example). Can these be scaled differently, without introducing an extra decade in the Y-axis?

We are focusing on the oxidized RO₂ (Ox_nRO₂) but the text and captions were not clear. We have revised them to make this clearer.

The following are the relevant changes to the manuscript and supplemental information.

All instances of “auto-oxidation” were changed to “autoxidation.”

In the abstract, it was clarified that the products of peroxy radical chemistry are resolved in the VBS.

Page 2, line 16, C^* plotting was clarified.

Section 3.1.3 RO_2 cross reaction kinetics was moved to after the following section and is now Section 3.1.4.

Page 9, line 18, the value of C_{ref}^o is defined.

Page 10, line 31, an indication that photolysis is “on” is given.

Page 11, line 17, the description of Figure 4 was clarified.

Page 12, line 10, the temperature dependence of the XVOC limits was described in more detail.

Page 12, line 28, language from the caption of Figure 5 was moved here to simplify the caption.

Page 14, the last paragraph was added to clarify Figure 9.

Figure 3, the y-limits on the top plot were adjusted.

Figure 4, the caption and the legend were made clearer.

Figure 5 and 6, the size of the 2D-VBS plots (top row) were adjusted.

Figure 5, caption language was moved into the discussion section.

Figure 7, the traces colors were changed.

Figure 8, y-limits were adjusted and the legend was made clearer.

Figure 9, the look of the monomer yield traces was changed and language was added to the caption to clarify the figure.

In the SI, typos in reactions 23, 24, and 26 were fixed.

In the SI, the section on the α_{OH} dependence was added.

Peroxy Radical Chemistry and the Volatility Basis Set

Meredith Schervish¹ and Neil M. Donahue¹

¹Center for Atmospheric Particle Studies, Carnegie Mellon University, 5000 Forbes Avenue, Pittsburgh PA 15213 USA

Correspondence: Neil M. Donahue (nmd@andrew.cmu.edu)

Abstract. Gas-phase ~~auto-oxidation~~autoxidation of organics can generate highly-oxygenated organic molecules (HOMs) and thus increase secondary organic aerosol production and enable new-particle formation. Here we present a new implementation of the Volatility Basis Set (VBS) that explicitly resolves peroxy radicals (RO₂) ~~formed via auto-oxidation~~products formed via autoxidation. The model includes a strong temperature dependence for ~~auto-oxidation~~autoxidation as well as explicit termination of RO₂, including reactions with NO, HO₂, and other RO₂. The RO₂ cross reactions can produce dimers (ROOR). We explore the temperature and NO_x dependence of this chemistry, showing that temperature strongly influences the intrinsic volatility distribution and that NO can suppress ~~auto-oxidation~~autoxidation under conditions typically found in the atmosphere.

1 Introduction

10 Atmospheric particles have dangerous health effects and influence the environment both through their direct scattering of incoming radiation and their indirect effect on clouds as cloud condensation nuclei. New-particle formation (secondary particle production) constitutes the largest source of particles in the atmosphere; furthermore many if not most particles with significant health or climate effects consist largely of secondary material, having grown via condensation from a much smaller initial size. Organic vapors contribute to both nucleation and growth of new particles as well as growth of primary nano particles, all
15 of which constitutes secondary organic aerosol (SOA). Especially for condensation to the smallest particles, the volatility of those condensible organics is important. Therefore it is of interest to investigate and model how volatile precursors oxidize in the atmosphere to low volatility or extremely-low volatility products (LVOCs and ELVOCs) that will contribute to SOA. Furthermore, organic oxidation products alone can drive “pure biogenic” nucleation (Kirkby et al., 2016), and so the formation mechanisms and nucleation rates of a new class of ultra-low volatility products (ULVOCs) that can drive nucleation is also of
20 interest.

One important class of condensible organics is the group known as highly-oxygenated organic molecules (HOMs). HOMs are ~~are~~ organic compounds containing at least six oxygen atoms formed through peroxy-radical (RO₂) isomerization and subsequent addition of molecular oxygen, which preserves RO₂ functionality in a recursive process known as ~~auto-oxidation~~autoxidation, followed by RO₂ termination to molecular products (Crouse et al., 2013; Ehn et al., 2014; Bianchi et al., 2019). HOMs open
25 up a rich space for gas-phase organic oxidation chemistry to strongly influence new-particle formation involving condensible organic products. Because the chemistry involves competition between internal isomerization (which typically will have

a relatively high energy barrier and thus a strong temperature dependence) and radical-radical termination reactions (which typically have low barriers and thus only a modest temperature dependence), we expect a strong temperature dependence to HOM formation. Furthermore, because NO_x (especially NO) can greatly shorten RO_2 lifetimes, we also expect a strong NO_x dependence to HOM formation. Finally, to the extent that RO_2 - RO_2 cross reactions between radicals from different organic precursors can be important, there may be a rich interplay among the oxidation mechanisms for a host of different organic compounds.

The volatility basis set (VBS) has been developed and used widely as a framework to represent, track, and model the oxidation of volatile organic precursors, the subsequent production of condensible products, and their evolution through multiple generations of oxidation chemistry and fragmentation (Donahue et al., 2005, 2006, 2011, 2012b, 2013; Chuang and Donahue, 2016). For numerical calculations, the 2D-VBS space is discretized into bins, with each $\text{C}^*(300\text{ K})$ bin typically separated by 1 order of magnitude and each O:C bin separated by 0.1. It is not necessary to know the identity of molecules in these bins, but this can be inferred by application of composition activity relations such as SIMPOL (Pankow and Asher, 2007). In general, the perspective of the VBS has been to explicitly track the most important observable properties of organics with respect to organic-aerosol formation – volatility ($\text{C}^*(\text{T})$) and the degree of oxidation (O:C) – forming the so-called two-dimensional volatility basis set (2D-VBS). Where specific products have known properties, those molecules can be located individually in the 2D-VBS. Where specific products are not known, the 2D-VBS can still track the overall carbon in a reactive system, with properties (C^* and O:C) evolving following known chemistry during photochemical aging. In this work, we plot everything using a $\text{C}^*(300\text{ K})$ x-axis so as to visualize how the products of the chemistry are changing rather and inferring how this would affect condensation.

The importance of RO_2 branching chemistry has so far been recognized implicitly in VBS formulations (Presto and Donahue, 2006; Henry and Donahue, 2011), but not explicitly. Instead, the product (volatility) distribution in the VBS has been based on some measure of the RO_2 branching (i.e. $\text{VOC}:\text{NO}_x$ or RO_2 branching in an explicit mechanism). Consequently, there have been “high- NO_x ” products and “low- NO_x ” products (volatility distributions) (Presto and Donahue, 2006), or even “high- HO_2 ” and “high- RO_2 ” products (Henry and Donahue, 2011), that can be mixed to form products at intermediate NO_x (or $\text{HO}_x:\text{RO}_x$) based on this indirect measure of RO_2 branching. Further, relatively little has been done to represent any temperature dependence of VOC oxidation in VBS implementations.

The purpose of this paper is to extend the 2D-VBS to explicitly represent RO_2 chemistry, including RO_2 oxidation and HOM formation as well as all forms of RO_2 termination, and only distribute products into volatility bins after RO_2 termination in an explicit gas-phase chemical mechanism. In this way we can represent the gas-phase HOM formation mechanism, its temperature dependence, and the rich array of competing RO_2 termination processes in a scheme that can merge seamlessly with any gas-phase chemical mechanism (MCM, etc.) while maintaining the generality of the VBS and its ability to represent the ongoing chemistry of organic species associated with organic aerosol formation and particle growth.

2 Background

HOMs and their properties have been measured in multiple laboratory and field studies. HOMs can drive pure biogenic nucleation indicating that, in the VBS context, at least some of them must be ELVOCs/ULVOCs. Stolzenburg *et al.* (Stolzenburg *et al.*, 2018) and Tröstl *et al.* (Tröstl *et al.*, 2016) report measurements of HOMs in the LVOC and SVOC range during experiments in the CLOUD chamber at CERN, showing that these HOMs (especially LVOCs) drive growth during new-particle formation, providing a significant reservoir of condensable species to stabilize particles after initial clustering (Stolzenburg *et al.*, 2018; Tröstl *et al.*, 2016). From these data, both collected under NO_x-free conditions, HOM products are expected to be distributed in SVOC, LVOC, and ELVOC range, with the largest concentration as LVOCs.

The composition and properties of HOMs produced during oxidation of a precursor such as α -pinene (as well as their quantitative yields) depend on the conditions under which they are formed. Frege *et al.*, again at CLOUD, found that at lower temperatures fewer total HOMs are formed, with dimers seeing the sharpest fall-off (Frege *et al.*, 2018). Lehtipalo *et al.* showed that increasing NO_x concentrations suppress the ELVOC HOMs but have less of an effect on the LVOC and SVOC HOMs (Lehtipalo *et al.*, 2018).

There are two important elements to HOM formation and their volatility distribution. The first is ~~auto-oxidation~~autoxidation itself, which produces progressively more oxidized peroxy radicals via H-atom transfer and thus -OOH functionalization before the radicals ultimately terminate to form stable products. The second is dimerization, which is one of the termination processes, where these functionalized RO₂ associate to form a covalently bonded dimer (presumably a peroxide, ROOR). The first process plays a key role in particle growth and the temperature dependence of condensable vapor yields. The second process may be rate limiting for pure biogenic nucleation.

~~Auto-oxidation~~Autoxidation involves an internal H-atom transfer, which almost certainly has a significant activation energy. Further, the process is observed to be competitive with bimolecular reactions on a timescale of 1 s or longer (Ehn *et al.*, 2014). Unimolecular reactions have an intrinsic rate constant (A-factor) given by molecular vibrational frequencies, and even loose bending modes in molecules have frequencies of THz. To slow down unimolecular reactions to 1 s⁻¹ or so, a high activation energy is thus almost essential. Rate coefficients for competitive reactions suggest an ~~auto-oxidation~~autoxidation energy barrier in the range of 15-18 kcal mol⁻¹ (7500-9000 K). This is also consistent with quantum chemical calculations as well as experimental data fitted to an extended MCM model (Rissanen *et al.*, 2014; Molteni *et al.*, 2019). This high activation energy also means that the RO₂ isomerization reactions will have a strong temperature dependence, becoming very slow at low temperature.

In contrast to the strong temperature dependence of ~~auto-oxidation~~autoxidation, the two canonical RO₂ loss reactions, with HO₂ and NO, both have only a weak temperature dependence with similar rate coefficients near 10⁻¹¹ cm³ molec⁻¹ s⁻¹ largely independent of RO₂ structure (Atkinson *et al.*, 2008). HO₂ levels typical in the lower atmosphere are roughly 3 pptv, or 10⁸ molec cm⁻³, giving a first-order low-NO_x loss frequency of 10⁻³ s⁻¹. NO in polluted areas can go much higher, increasing the high-NO_x loss to 0.1 s⁻¹ or even higher. This establishes the competitive range for RO₂ first-order loss in the 0.001 - 1 s⁻¹ range in the atmosphere. Because these rate coefficients are only weakly sensitive to temperature, the high activation energy for

the H-atom transfer in ~~auto-oxidation~~autoxidation means we expect the reactions with HO₂ and NO to be more competitive at low temperature.

Another RO₂ loss is to react with other RO₂. Unlike their reactions with HO₂ and NO, in which the rate coefficients depend only weakly on the nature of the R group, the rate coefficients for RO₂-RO₂ self and cross reactions are extremely sensitive to the nature of the R group. This has been well established for decades for the self reactions of different small RO₂ (Madronich and Calvert, 1990; Donahue and Prinn, 1990; Wallington et al., 1992; Tyndall et al., 2001). However, because ambient RO₂ concentrations rarely exceed ambient HO₂ (Mihelcic et al., 2003; Tan et al., 2018), reactions with other RO₂ will only be a major RO₂ loss pathway in the atmosphere when the rate coefficient equals or exceeds 10⁻¹¹ cm³ molec⁻¹ s⁻¹. This is in contrast to low-NO_x chamber experiments, where RO₂ concentrations can greatly exceed HO₂ concentrations, potentially biasing the chambers away from reactions important in the atmosphere.

At least for highly oxygenated peroxy radicals, association to form dimers has been found in some experimental studies to proceed with a rate coefficient near the collisional limit ($k > 10^{-10}$ cm³ molec⁻¹ s⁻¹) (Berndt et al., 2018; Molteni et al., 2019). However Zhao *et al.* find that the typical rate coefficient for presumably similar RO₂ + RO₂ association reactions is at least an order of magnitude slower (Zhao et al., 2017). These findings may or may not be directly in conflict given the wide range of peroxy-radical rate coefficients. The general tendency is that electron withdrawing groups (i.e. acyl groups in peroxy acyl radicals) increase the RO₂ self reaction rate coefficients while electron donating groups (i.e. t-butyl in t-butyl peroxy radicals) lower the rate coefficients. Thus, very fast cross-reaction rate coefficients for highly oxygenated RO₂ radicals is consistent with the general trend.

~~Auto-oxidation~~Autoxidation includes a unimolecular hydrogen shift reaction in which a peroxy moiety abstracts a hydrogen elsewhere on the molecule, generating an alkyl radical, which molecular oxygen will add to in turn, regenerating a peroxy radical functionality on a now more-oxidized carbon backbone. This process is significant in its ability to rapidly generate multi-functional oxygenation products in only a single “generation” of chemistry (stable molecule to stable molecule). However, experimental and theoretical evidence suggests that not every peroxy radical is readily capable of undergoing ~~auto-oxidation~~autoxidation. The fraction of peroxy radicals that will auto-oxidize will be different depending on the precursor of interest; for α-pinene three of the four peroxy radicals from ozonolysis can auto-oxidize. Ehn *et al.* found that the yield of highly oxidized peroxy radicals from OH oxidation of α-pinene was lower than from ozonolysis, indicating that while OH radical-derived peroxy radicals can auto-oxidize, the process is either slower or there are fewer that auto-oxidize readily (Ehn et al., 2014).

To summarize, three important characteristics of a “strongly auto oxidizing” system such as O₃ + α-pinene are emerging. First, most of the products under atmospheric conditions are likely to be “traditional” oxidation products formed without an ~~auto-oxidation~~autoxidation step. Second, the amount of ~~auto-oxidation~~autoxidation is likely to be strongly temperature dependent, with more at higher temperature. Third, some termination of at least the highly oxygenated RO₂ results in covalently bound (and highly oxygenated) dimers, which will have extraordinarily low vapor pressures.

Each consequence has an important implication, which we give in reverse order. First, the dimerization may be the rate-limiting step for “pure organic” nucleation; because it involves a cross reaction, this means that organic nucleation may also be

highly sensitive to interactions between different hydrocarbon oxidation sequences, especially at low NO_x . It remains somewhat unclear how important this termination is in the real atmosphere vs chambers, given the high $\text{RO}_2:\text{HO}_2$ in chambers; however, the characteristic dimer products are observed in the atmosphere. This strongly suggests that these association reactions are important in the atmosphere.

5 Second, the temperature dependence of the monomer ~~auto-oxidation~~autoxidation products may well be counterbalanced by the simple temperature dependence of vapor pressures. Both of these govern organic condensation, especially to very small particles. Consequently, particle growth rates from organic oxidation (as well as secondary organic aerosol mass yields) are likely to be less sensitive to temperature than one would otherwise expect. They are also likely to be less sensitive to interactions between different hydrocarbon oxidation sequences. Particle nucleation and growth thus may be partially decoupled, making
10 treatment of each separately important, especially in the “valley of death” region below 3-5 nm where highly diffusive particles are most vulnerable to coagulation loss.

Third, the large majority of organic oxidation products are likely to be oxygenated species with lower vapor pressure than the precursor that remain in the gas phase (“traditional” SVOCs). Later-generation chemistry of these products remains an important topic that can not be forgotten (Donahue et al., 2005, 2012a); these subsequent steps have already been shown to
15 themselves be efficient sources of HOMs (Schobesberger et al., 2013; Ye et al., 2018).

3 The model

For this work we will model an idealized batch reactor with oxidation of α -pinene leading to HOM products. The model is split into two pieces: a general chemical mechanism and a specific implementation for the batch reactor. Here we only simulate the gas-phase chemistry, culminating in formation (and loss) of RO_2 species, with RO_2 termination mapping into the 2D-VBS
20 via a succession of kernels specific to each termination step.

3.1 Chemical mechanism

The model we use here is an explicit gas-phase photochemical box model using a custom written perl mechanism parser that produces Matlab code for the coupled differential equations describing an arbitrary set of input reactions. The reaction set here is relatively standard small-molecule HO_x chemistry with added α -pinene. We list the full set of reactions and rate coefficients
25 in the supplemental material.

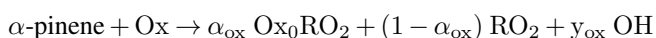
The reactions begin with oxidation of a precursor, in this case α -pinene via ozonolysis, OH, and the nitrate radical (when NO_x is present). Most of the products of these oxidation reactions will be peroxy radicals, with 10 carbons each, which will undergo two types of reactions: ~~auto-oxidation~~autoxidation or radical termination. ~~Auto-oxidation~~autoxidation, as described previously, is a unimolecular reaction followed by O_2 addition that generates a more oxidized peroxy radical that will have the
30 same reaction pathways available to it again as the parent RO_2 . It is thus effectively recursive. The radical termination reactions available to a peroxy radicals are reaction with HO_2 , NO, or another peroxy radical.

It is likely that peroxy radicals have a diversity of H-transfer activation energies (and A-factors), and that this diversity is important to the overall system behavior. We currently lack sufficient kinetic information to constrain this, and so we adopt a simple approach. For the initial RO₂ (without additional -OOH functionality), we assume that some fraction can undergo ~~auto-oxidation~~autoxidation and the remainder cannot (it is a binary choice). All of the RO₂ that can auto oxidize does so with a single barrier height and A-factor, and this is common to all of the subsequent oxidized RO₂.

A second complication is the role of alkoxy radicals (RO), which can be chain propagating (including a much more widely recognized 1-4 H shift that is broadly similar to the H shift in ~~auto-oxidation~~autoxidation) (Atkinson, 1997; Lim and Ziemann, 2009) However, for this set of simulations only we shall assume that RO radicals effectively terminate to molecular products; that is consistent with our broad objective to upgrade the 2D-VBS from simply generating (NO_x dependent) products from a precursor (i.e. α-pinene) to allow the products to be controlled by peroxy radicals. In the future we shall relax this assumption and permit regeneration of RO₂ from RO.

3.1.1 α-pinene reactions

We are simulating α-pinene ozonolysis but this chemistry will produce OH radicals and, with added NO_x, NO₃ as well. Consequently, we have three oxidants to consider. It has been found that OH oxidation of α-pinene produces far fewer HOMs than O₃ (Kirkby et al., 2016), presumably because the OH addition does not immediately cleave the 6-member ring in α-pinene. Further, oxidation of α-pinene by NO₃ has been shown to produce very little first-generation SOA (Fry et al., 2014; Ng et al., 2017). However, almost all primary oxidation results in peroxy radicals (with the exception of some small fraction of stabilized Criegee Intermediates), though only some of those may have rapid ~~auto-oxidation~~autoxidation pathways. To address this, we assign two first-generation RO₂ radicals to each oxidation pathway; one, O_{x0}RO₂, has the potential for ~~auto-oxidation~~autoxidation, while the second, RO₂, does not.



Here we assume that $\alpha_{\text{O}_3} = 0.25$, $\alpha_{\text{OH}} = 0.1$, and $\alpha_{\text{NO}_3} = 0$. Further, $y_{\text{O}_3} = 0.8$ (Presto and Donahue, 2004), $y_{\text{OH}} = 0$, and $y_{\text{NO}_3} = 0$.

3.1.2 ~~Auto-oxidation~~Autoxidation

The ~~auto-oxidation~~autoxidation process involves an internal H-atom transfer in an RO₂ radical, immediately followed by O₂ addition to reform a new RO₂ radical with an added -OOH group. Broadly, we label these reactions



where n is the number of -OOH groups (the number of generations of ~~auto-oxidation~~autoxidation). The rate-limiting kinetic parameter is the unimolecular rate constant for H-atom transfer, which we express as an Arrhenius rate coefficient with a pre-

exponential $A = 10^8 \text{ s}^{-1}$ for the Ox_0RO_2 , which decreases to $A = 7 \times 10^7$ and $A = 6 \times 10^7$ for the Ox_1RO_2 and the Ox_2RO_2 respectively, and an activation energy $\theta_a = 7500 \text{ K}$ that is consistent for all [auto-oxidation-autoxidation](#) steps in our base-case simulation. This gives an H-atom transfer rate coefficient for Ox_0RO_2 of 0.01 s^{-1} at 298 K and 10^{-7} s^{-1} at 248 K for the Ox_0RO_2 . Raising the activation energy to $\theta_a = Ea/R = 8000 \text{ K}$ gives an H-atom transfer rate coefficient of $2 \times 10^{-4} \text{ s}^{-1}$ at 298 K and $7 \times 10^{-7} \text{ s}^{-1}$ at 248 K. Even though each H-atom transfer step proceeds with different rate coefficients, we are still likely missing a large amount of the diversity of barriers and rate constants. In addition it is plausible that the barriers drop with increasing extent of [auto-oxidation-autoxidation](#).

There are multiple peroxy radical structures formed both initially and via every [auto-oxidation-autoxidation](#) reaction. Furthermore, HOM RO_2 radicals with multiple -OOH groups can rapidly interconvert, and even the exact same peroxy radical can react with other radicals to produce different product structures. This leads to a large and complex distribution of final product structures. In order to reduce this complexity, we represent the peroxy radicals as individual surrogate molecules – points in the 2D-VBS space – with [auto-oxidation-autoxidation](#) moving surrogate to lower volatility and higher O:C. We thus explicitly represent the volatility of the RO_2 radicals, which we show in Figure 1 as a sequence of four colored circles (along with α -pinene itself as a red circle), ranging from light green for all “traditional” RO_2 that have not undergone [auto-oxidation-autoxidation](#) through a succession of deeper green colors for Ox_nRO_2 that have undergone $n = 1\text{-}3$ generations of [auto-oxidation-autoxidation](#).

3.1.3 RO_2 cross reaction kinetics

Based on the available evidence that RO_2 self reaction rate constants accelerate with the presence of electron withdrawing functional groups near the -OO moiety, we assume that the self reaction rate constants for the Ox_nRO_2 are given by-

$$\text{RO}_2 \text{ } k_{n,n} \text{ cm}^3 \text{ molec}^{-1} \text{ s}^{-1} \text{ } \text{RO}_2 \text{ } 1.0 \times 10^{-13} \text{ } \text{Ox}_0\text{RO}_2 \text{ } 1.0 \times 10^{-13} \text{ } \text{Ox}_1\text{RO}_2 \text{ } 1.0 \times 10^{-12} \text{ } \text{Ox}_2\text{RO}_2 \text{ } 1.0 \times 10^{-11} \text{ } \text{Ox}_3\text{RO}_2 \text{ } 1.0 \times 10^{-10}$$

Given the enormous number of possible cross reactions (and paucity of kinetic data) Madronich (Madronich and Calvert, 1990) proposed a simple parameterization to estimate the cross-reaction rate coefficient for two dissimilar RO_2 radicals as the geometric mean of their self reaction rate constants, $k_{n,m} = 2 \sqrt{k_{n,n} k_{m,m}}$. The factor of 2 is due to the different symmetry of the self and cross reactions.

3.1.3 Unimolecular RO_2 termination

Peroxy radicals may undergo unimolecular termination at any point in the [auto-oxidation-autoxidation](#) chain, but exact barrier height and pre-factors for these reactions remain unknown. For example, radical termination may occur via OH loss following a H-abstraction from a carbon with an -OOH group attached. Assuming that the termination involves a bond scission and potentially an H-transfer between neighboring groups, this termination is likely to have a higher A-factor but a higher activation energy than the internal isomerization (which has a long cyclic transition state and thus a relatively low A-factor). Here we represent this process with a pre-factor of 10^{15} s^{-1} and a barrier of 13000 K. This gives a termination rate coefficient of 10^{-4} s^{-1} at 298 K and $1.7 \times 10^{-8} \text{ s}^{-1}$ at 248 K. As with [auto-oxidation-autoxidation](#), there is every reason to believe that different

functional groups on the peroxy radical would hinder or enhance the unimolecular termination pathway, but we use a consistent pre-factor and barrier for every peroxy radical to represent a complicated reaction pathway more simply.

In our framework, unimolecular termination products are treated as “monomer” products previously discussed. They may or may not be HOMs depending on whether the peroxy radical that produced them underwent ~~auto-oxidation~~ autooxidation to any extent.

3.1.4 RO₂ cross reaction kinetics

Based on the available evidence that RO₂ self reaction rate constants accelerate with the presence of electron withdrawing functional groups near the -OO moiety, we assume that the self reaction rate constants for the O_x_nRO₂ are given by

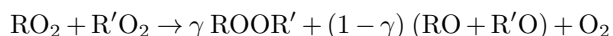
<u>RO₂</u>	<u>k_{n,n}</u> <u>cm³ molec⁻¹ s⁻¹</u>
<u>RO₂</u>	<u>1.0 × 10⁻¹³</u>
<u>O_{x0}RO₂</u>	<u>1.0 × 10⁻¹³</u>
<u>O_{x1}RO₂</u>	<u>1.0 × 10⁻¹²</u>
<u>O_{x2}RO₂</u>	<u>1.0 × 10⁻¹¹</u>
<u>O_{x3}RO₂</u>	<u>1.0 × 10⁻¹⁰</u>

10 Given the enormous number of possible cross reactions (and paucity of kinetic data) Madronich (Madronich and Calvert, 1990) proposed a simple parameterization to estimate the cross-reaction rate coefficient for two dissimilar RO₂ radicals as the geometric mean of their self reaction rate constants, $k_{n,m} = 2 \sqrt{k_{n,n} k_{m,m}}$. The factor of 2 is due to the different symmetry of the self and cross reactions.

3.1.5 RO₂ dimerization

15 The mechanism for RO₂ dimerization is unknown. It is a theoretical puzzle because RO₂ reactions are thought to proceed through a weakly bound “tetroxide” intermediate, ROO-OOR, which is a singlet closed-shell species (Lee et al., 2016). If by whatever (presumably multiple step) process this singlet species eliminates molecular oxygen, O₂(³Σ), the singlet peroxide ROOR is spin forbidden. In the more common radical pathway, which produces RO + RO + O₂, the two RO radicals are spin entangled in a triplet state. They cannot re-combine into a peroxide (ROOR) without first crossing to the singlet state.

20 Here we model the RO₂ cross reactions as



with “products” being treated as stable molecules within the Volatility Basis Set. A more general treatment would also include both the radical (RO) and molecular (alcohol + carbonyl) pathways, which are treated with a branching ratio β (Tyndall et al.,

2001); here we assume that $\beta = 1$ for all of these peroxy radicals, consistent with findings that the radical pathway is favored for peroxy radicals with electron withdrawing functional groups near the -OO moiety.

It may be that the ability to form dimers is directly dependent on additional functional groups in the RO₂ molecules, or it may be an indirect consequence, for example related to volatility and possibly cluster lifetime when two RO₂ radicals interact.

5 Because we are explicitly tracking the volatility of the RO₂ radicals produced via ~~auto-oxidation~~autoxidation (and because some have very low volatility), here we shall explore the possibility that dimerization is somehow tied to the volatility of the reacting RO₂ radicals. Specifically, we hypothesize that when low volatility RO₂ species collide they will form a short-lived (radical) cluster, both before and after reacting. We further assume that ROOR dimer formation in this cluster follows the more traditional radical (RO) step, and that the product cluster must be long enough lived for collisions with air molecules to induce
10 a spin flip in the initially triplet entangled system. As a rough measure of cluster lifetime we will use the geometric mean volatility of two interacting RO₂ species (i.e. the average of the $\log C^\circ$ values).

If dimerization is volatility dependent, the probability of dimerization occurring when two peroxy radicals interact may be approximated by:

$$\gamma = \frac{1}{1 + C_{GM}^\circ / C_{ref}^\circ} \quad (1)$$

15 where C_{GM}° is the geometric mean of the effective saturation concentrations of the two reacting peroxy radicals and C_{ref}° is a temperature dependent reference saturation concentration representing where we expect half of the reacting peroxy radicals to dimerize. The value of C_{ref}° used in this work is 10^{-2} at 298 K and moves 1 order of magnitude lower in volatility per 10 K reduction in temperature. In our base case we assume a rate coefficient for highly oxidized α -pinene peroxy radical reactions near the collisional limit, but given the branching ratio in Eq. 1 the dimerization product yield can be much lower (depending
20 on RO₂ volatility).

3.2 RO₂ termination kernels and the VBS

Following α -pinene oxidation, the initial, “traditional” RO₂ is a di-carbonyl peroxy radical (C₁₀H₁₅O₄). Each carbonyl functional group reduces the volatility by about one order of magnitude (Pankow and Asher, 2007), and we assume that the -OO moiety decreases the volatility by roughly another 1.5 orders of magnitude; consequently, this RO₂ has a ~~$C^\circ(300) \simeq 10^4$~~
25 $C^\circ(300K) \simeq 10^4$ $\mu\text{g m}^{-3}$. Each successive Ox_{*n*}RO₂ differs from its predecessor by having an additional -OOH functional group. These nominally decrease volatility by 2.5 orders of magnitude (Pankow and Asher, 2007); however, there is evidence that multifunctional molecules with opportunities for internal hydrogen bonding have higher volatilities than simple composition activity relations suggest (Kurtén et al., 2016). To crudely represent this we assign ~~$C^\circ(300) \simeq 10$~~ $C^\circ(300K) \simeq 10$ $\mu\text{g m}^{-3}$ for Ox₁RO₂ but assume that each successive generation of ~~auto-oxidation~~autoxidation decreases volatility by only 2 orders of
30 magnitude, as shown in Figure 1. It is interesting to note that Ox₂RO₂ on up the ~~auto-oxidation~~autoxidation sequence have a low enough volatility that they are likely to remain in particles if they collide with them.

Figure 1 also shows the broad “XVOC” ranges as colored bands. This includes the new ULVOCs in purple, which have a sufficiently low volatility ($C^\circ(T) \leq 3 \times 10^{-9} \mu\text{g m}^{-3}$) to nucleate efficiently under typical conditions (it is supersaturation that ultimately drives this). The ELVOCs, in contrast, will stick to any particle of any size they hit, but may not contribute significantly to nucleation itself (in practice it may be the geometric mean of $C^\circ(T)$ for two colliding vapors that governs
5 nucleation, just as we hypothesize for ROOR formation).

We represent RO_2 termination reactions to products as kernels anchored to the peroxy radical point that produced them. These kernels allow us to represent a wide variety of stabilization pathways producing a wide variety of different products through one surrogate species; the variety of species that the surrogate represents are instead mapped to a distribution of products within the 2D-VBS defined by a transformation relative to the surrogate RO_2 volatility and O:C. In Figure 1 we
10 show the sum of these kernels (weighted by branching) for the three broad classes of products defined earlier: “traditional” oxidation products, monomers involving at least one generation of ~~auto-oxidation~~autoxidation, and ROOR dimers. We provide the individual kernels (relative to the C° and O:C values for each RO_2) in the supplemental material. The net effect is a concentration of traditional products with O:C modes in the SVOC and IVOC range, which in earlier VBS parameterizations of α -pinene SOA have constituted all of the products (Presto and Donahue, 2006; Jimenez et al., 2009; Donahue et al., 2012b),
15 augmented by a tongue of HOM monomer products extending through the LVOC range and up to O:C > 1, and finally with a parallel shoal of HOM dimer products spanning the ELVOC range and extending into the ULVOC range (causing “pure biogenic” nucleation (Kirkby et al., 2016)).

We fully resolve the reaction products and then take the final concentration of every surrogate species (for example “ $\text{O}_{x_2}\text{RONO}_2$ ” represents all organonitrates derived from second-generation auto-oxidized peroxy radicals) and map those to a distribution of
20 products in the 2D-VBS using the appropriate kernel. This can readily be adapted to form a module (operator) within a larger framework representing particle microphysics, transport, wall loss, etc.

3.3 Ideal reactor

Here we model an ideal batch reactor with an initial input of precursor α -pinene that is oxidized over time leaving only stable oxidation products, with essentially no precursor remaining at the end of the simulation. There is no wall loss, ventilation,
25 additional vapors added after the initialization, nor particle condensation or nucleation; our goal here is to just probe the chemistry of interest without interference of the physics of typical chamber experiments. We present results varying the temperature, NO_x and barrier-height dependence of the yields of α -pinene ozonolysis. We simulate 600 ppt of α -pinene ($1.5 \times 10^{10} \text{ molec cm}^{-3}$) reacting with 40 ppb of ozone, which corresponds to a lifetime of approximately 4 h ($1.4 \times 10^4 \text{ s}$) at 298 K. When we simulate NO_x chemistry we add the NO_x to the system as NO, after which it undergoes reaction to NO_2 and reaches an
30 equilibrium ratio of $\text{NO}:\text{NO}_2 \simeq 1:10$. The value we report as the concentration of NO_x is the amount of NO initially added into the system. [All the simulations here are run in light so that photochemistry is able to occur.](#)

4 Results

We present results showing the final products of the chemistry described above and how they resolve within the 2D-VBS. We make qualitative comparisons with previous experimental results to show the validity of our approaches.

4.1 Base-case run

5 We will start with a “base-case” run at 298 K without NO_x to demonstrate the model and its output. As the α -pinene reacts, the peroxy radicals quickly build up to a steady state and then decay in consort with the α -pinene as they auto-oxidize and form stable products. As Figure 2 shows, each of the successively more oxidized peroxy radicals reaches a maximum concentration at a similar time, but to progressively lower maximum values. The stable products are formed via the various peroxy radical termination processes and in this simulation they have no sinks and so simply accumulate. Their yields are thus simply their
10 final concentrations divided by the initial α -pinene concentration.

In Figure 3a we show one such set of terminal products, labeled Ox_n to indicate the number of ~~auto-oxidation~~autoxidation steps. These products form from both $\text{RO}_2 + \text{NO}$ and $\text{RO}_2 + \text{RO}_2$ reactions and so scale with the RO_2 radicals themselves, but because they are not lost in the batch reaction (here we do not simulate aging with the 2D-VBS) their concentrations accumulate over time.

15 In Figure 3b we show the corresponding dimer (ROOR) concentrations. We identify the dimers by a number pair (n, m) indicating the ~~auto-oxidation~~autoxidation extent of the associated Ox_nRO_2 . Here the situation is more nuanced because the dimers are formed exclusively through cross reactions and we assume (Eq. 1) that the dimer yields depend on the RO_2 volatility. Consequently, even though the most oxidized RO_2 have lower concentrations, they produce dimers with higher yields. The 2-2 and 3-3 symmetric dimers, along with the 2-3 cross dimer, are the most abundant.

20 The ultimate product distribution is dependent on the competition between ~~auto-oxidation~~autoxidation and termination via other radical species. Thus it is important to fully implement HO_x and NO_x chemistry and it is informative to see how the concentrations of these radicals vary throughout the simulation. We show HO_2 and NO for various levels of added NO_x in Figure 4, along with the sum of oxidized RO_2 ($\sum \text{Ox}_n\text{RO}_2$). Characteristically for chamber experiments, HO_2 remains at a low level ($\lesssim 10^7$ molec cm^{-3}) compared to the atmosphere due to the relative scarcity of species such as CO and CH_2O that
25 directly convert OH into HO_2 and also photolyze to produce HO_2 . Thus HO_2 remains far rarer than even the OxRO_2 while most α -pinene is oxidized, with $\text{OxRO}_2:\text{HO}_2 \simeq 40$ ~~and as shown in Figure 4. Including the RO_2 that wasn't oxidized, shown in Figure 2, then we increase that ratio,~~
30 all $\text{RO}_2:\text{HO}_2 \simeq 80$. Because in our simulation we add NO_x as NO , at first the NO levels drop rapidly via reaction with HO_2 and RO_2 , but then reach a steady state as NO_2 photolysis replenishes NO . In general for batch chamber experiments, NO_x is not added at the steady-state $\text{NO}:\text{NO}_2$, and it is common to add NO as we simulate here; the rapidly evolving NO concentrations complicate interpretation of the results as the conditions can move from “high NO ” early in the experiment to “low NO ” later on. However, in this simulation, for 100 pptv added NO_x the NO stabilizes near 3 pptv. This is sufficient to slightly suppress the HO_2 , more significantly reduce the oxidized RO_2 , and to dominate RO_2 termination.

The OxRO₂ curves in Figure 4 allow one to assess RO₂ termination in general, remembering that the rate coefficients for HO₂ and NO termination are similar and (in our model) the OxRO₂ self reaction rate coefficients are up to ten times faster. This means that HO₂ is never an important RO₂ sink under these conditions, while NO becomes competitive between 50 and 100 ppt added NO_x (the NO concentration must be 10 times higher than the OxRO₂ to compete). Increasing NO significantly suppresses OxRO₂ and so by 1000 ppt NO_x the NO pathway is dominant at all times.

4.2 Temperature dependence

The temperature dependence of the HOM formation chemistry is a key diagnostic with great atmospheric significance. Experimental data indicate that HOM yields decrease with decreasing temperature and that HOM dimers especially follow this trend. This does not mean that condensible LVOC products necessarily decrease as products with a higher $C^\circ(300) - C^\circ(300K)$ will condense when it is cold; the XVOC color patches in the 2D-VBS figures show this volatility temperature dependence. Each XVOC region shifts to higher $C^\circ(300K)$ at lower temperatures meaning that a compound with a $\log(C^\circ(300K)) = -4$ would be in the LVOC range at 298 K, the ELVOC range at 278 K, and the ULVOC range at 248 K. However since essentially all of the (room temperature) ULVOCs and ELVOCs are dimers, their yields will follow the dimer trends.

In Figure 5 we show the temperature dependent results for our base-case NO_x-free simulation. Each column is a different temperature (248, 278, and 298 K). The top row is a 2D-VBS contour plot of the products, recapitulating Figure 1 with the volatility classes (defined by $C^\circ(T)$) shifting with temperature following Stolzenburg (Stolzenburg et al., 2018). The middle row is a 1D-VBS plot (summing the top plots over O:C) with histograms of carbon yields in each volatility bin, colored by the RO₂ termination process (NO, dimerization, HO₂, etc). The bottom row is color coded by the generation of ~~auto-oxidation~~ autooxidation, with darker colors corresponding to products of RO₂ that have undergone more ~~auto-oxidation~~ autooxidation steps.

In the bottom row of Figure 5 we can clearly see that the amount of products formed from auto-oxidized peroxy radicals decreases with decreasing temperature to the point where at 248 K, there is no significant contribution of ~~auto-oxidation~~ autooxidation to the yields at all. This is expected from the temperature dependence of the ~~auto-oxidation~~ autooxidation rate coefficient and the trend is supported with experimental data. In the middle plots, we see a reduction in HOM monomers at lower temperatures, but because the volatility classes shift toward higher $C^\circ(300) - C^\circ(300K)$ at lower temperature, there are still relatively high LVOC yields, which is consistent with previous growth rate measurements indicating large contributions from LVOCs to growth even at low temperature. We also see that at lower temperatures dimer yields are greatly reduced. This makes sense based on the hypothesis that when two peroxy radicals react the probability that they formed a dimer is dependent on their volatility, and thus dependent on the extent of autooxidation. However, at 248 K, we see an emergence of non-HOM dimers, dimers formed via reaction between two non-auto-oxidized peroxy radicals. These are "non-HOM" dimers as the definition of "HOMs" requires there to be an ~~auto-oxidation~~ autooxidation step in the formation process. They are a consequence of our hypothesis that dimer formation is related to RO₂ complex lifetime, as expressed in Eq. 1; any temperature dependence of dimer yields (and their O:C) is thus a test of this hypothesis.

In addition, we see almost no formation of products from an $\text{RO}_2 + \text{HO}_2$ pathway. This is not a major pathway for peroxy radical termination at any temperature, given our base-case assumption of a fast $\text{RO}_2 + \text{RO}_2$ reaction and the high $\text{RO}_2:\text{HO}_2$ in low- NO_x chamber conditions. There is however a slight temperature dependence of hydroperoxide formation as at low temperatures (with no NO_x) there is a larger build-up of the OX_0RO_2 , which have a relatively slow self reaction rate constant and thus do terminate with HO_2 .

4.3 NO_x dependence

Experimental data indicate that ULVOC/ELVOC yields are strongly reduced with increasing NO_x while LVOC and SVOC yields are less affected. In addition, at intermediate NO_x concentrations, HOM organo-nitrates will be formed contributing HOMs in the SVOC to LVOC range not found under low- NO_x conditions.

10 We show the NO_x dependent results for our 298 K simulation in Figure 6, which follows the temperature-dependent Figure 5 in form. Each column is a different NO_x concentration (50, 100, and 1000 ppt), but the results show the same qualitative pattern as those in Figure 5, with high NO_x taking the place of low temperature. NO suppresses ~~auto-oxidation~~autoxidation and HOM formation just as low temperature does, but “normal” hydroperoxides (formed via HO_2 termination) are replaced by organonitrates. Further, because the temperature is not reduced, the high- NO_x products remain largely in the SVOC class, so
15 high NO_x will suppress nucleation.

At very low NO_x (< 20 ppt), we see relatively little effect on yields, either type or ~~auto-oxidation~~autoxidation, compared to the zero- NO_x 298 K results in Figure 5. There is, however, some suppression of dimers. In our simulation, NO_x becomes competitive with ~~auto-oxidation~~autoxidation around 500 ppt and completely overpowers ~~auto-oxidation~~autoxidation around 1000 ppt. This is based on an $\text{RO}_2 + \text{NO}$ rate coefficient of $10^{-11} \text{ cm}^3 \text{ molec}^{-1} \text{ s}^{-1}$ and an activation barrier to ~~auto-oxidation~~autoxidation
20 ~~producing at~~autoxidation producing a rate coefficient of about 10^{-3} s^{-1} at 298 K. In this simulation we do not incorporate any variation in kinetics with the RO_2 classes (e.g. the isomerization activation energy) other than the dependence of dimerization on the geometric mean of RO_2 volatility expressed in Eq. 1 and the small change in the pre-factor for ~~auto-oxidation~~autoxidation discussed in section 3.1.2. Therefore we caution against making quantitative comparisons to experimental results such as Zhao et al., who found that competition between ~~auto-oxidation~~autoxidation and NO_x termination begins to favor the
25 NO_x pathway at about 20 ppbv of NO_x . It is highly likely that the RO_2 kinetics vary considerably depending on the exact RO_2 structure and very possible that more of this will need to be represented to obtain quantitative agreement with experimental observations.

In Figure 7 we show the NO_x effects on HOM monomers and dimers at different temperatures. For the NO_x range we simulate here, the major effect of NO is to suppress the total HOMs uniformly by roughly a factor of 10. In this plot we see
30 that while temperature has a relatively uniform effect of suppressing HOM monomers and dimers, NO_x suppress dimer yields more aggressively than it does HOM monomer yields. This can be explained due to the emergence of HOM nitrates, which are included in the monomer yields, as well as the consequence of NO reducing total OxRO_2 and thus the rate of peroxy radical association reactions.

It is important to note that the relatively low HO₂ concentrations in these runs may be enhancing the importance of NO_x chemistry here. With higher HO₂ concentrations, the RO₂ + HO₂ reaction will compete with the RO₂ + NO and reduce the nitrate yields. However, the HO₂ concentrations simulate here line up with what is often seen in very clean chamber experiments and thus our NO_x conclusions hold for those cases.

5 4.4 Sensitivity studies

As stated, the energy barrier to ~~auto-oxidation~~-autoxidation is an important unknown in this model. It is constrained experimentally by the competition with the RO₂ + NO reaction, but the coefficient associated with ~~auto-oxidation~~-autoxidation could span orders of magnitude for different peroxy radicals. In all the simulations described so far, we used a single barrier for ~~auto-oxidation~~-autoxidation for every peroxy radical, and reduced the pre-factor as n , the extent of ~~auto-oxidation~~autoxidation,
10 increased.

We employ two methods to investigate the barrier height dependence look at the yields: fixing the rate coefficient at 298 K and varying its activation energy (in a Clausius-Clapeyron like expression) and allowing the rate coefficient to vary within an order of magnitude of what was used in the “base-case” scenario over the whole temperature range. This is to see the effect of the ~~auto-oxidation~~-autoxidation barrier height on the HOM and dimer yields as well as to provide a context for the error
15 associated with our assumption regarding the barrier height. The effect of these methods on the ~~auto-oxidation~~-autoxidation rate constant is shown in the Supplemental Information.

As shown in Figure 8, changing the barrier height strongly affects the calculated amount of ~~auto-oxidation~~autoxidation, especially at low temperatures. There is little effect near 298 K because that is where we prescribe the rate coefficient. In Figure 9, we show results from allowing the rate coefficient to vary an order of magnitude over the entire temperature range,
20 producing dimer and monomer yields that span orders of magnitude. The solid curves indicate the base-case scenario described above. This allows us to put some bounds on the rate coefficient of ~~auto-oxidation~~-autoxidation as experimentally dimer and monomer yields fall well within the shaded region of the plot.

There is ample evidence in the kinetic literature for a high degree of variability in the autoxidation rate. Therefore, it is possible that to adequately describe autoxidation, its effects on new-particle formation as well as SOA formation, and the sensitivity of both to NO, T, HO₂, etc, we will need to treat “fast?” and “slow?” reacting RO₂. While it is possible for us to put bounds on autoxidation with the assumptions made here, it is very likely that the autoxidation of specific peroxy radicals lie outside these bounds. For example, the low barrier shown in Figure 9 is likely outside these bounds as at the highest temperatures the monomer yields are lower than the dimer yields, which contradicts experimental evidence. However, with relatively minor changes to other parameters (e.g. the dimerization rate coefficient, the branching ratio to dimers γ , the unimolecular termination rate coefficient), this barrier height would be completely reasonable and therefore still represents a
30 good lower bound for the auto-oxidation barrier height. The “Ox_nRO₂” represent a variety of peroxy radicals and therefore these bounds are representative of the general behavior of these peroxy radicals rather than being bounds for any specific peroxy radical species.

4.4.1 NO_x dependence of temperature dependence

We also want to investigate how the similar trends of decreasing temperature and increasing NO_x work together. The bottom plot of Figure 10 clearly shows this synergistic effect on ~~auto-oxidation~~autoxidation, as products that have undergone any ~~auto-oxidation~~autoxidation are almost completely suppressed at the highest NO_x concentration and the lowest temperature investigated here. The top plot of Figure 10 shows once again that decreasing temperature and increasing NO_x work together to suppress both HOM monomers and HOM dimers as well as a few other trends. As NO_x is increased, the yield of nitrates increases, but at any specific NO_x concentration the amount of nitrate formed is effectively temperature-independent. However, HOM nitrates are only formed at the highest temperature and at lower NO_x concentrations; obviously, to form nitrates some NO_x needs to be present, but if too much is present, the peroxy radicals will terminate before they can auto-oxidize to form HOM nitrates. At low NO_x concentrations the HOM formation is dependent on temperature as discussed previously, but at high NO_x concentrations the yields are completely dominated by termination with NO. We can also see at low NO_x and low temperatures, the appearance of non-HOM dimers; formation of these less oxidized peroxides is a consequence of our assumption that a long-lived RO₂ molecular cluster is required to allow the products to cross to the singlet spin surface. This plot also shows the temperature and NO_x dependence of yields from the RO₂ + HO₂ reaction. While never a large portion of the total yield, products of this reaction increase under low temperature and low NO_x conditions. When the temperature is low, most of the peroxy radicals present are Ox₀RO₂, which based on our association rate constants, will react the slowest with each other. This allows for more of the peroxy radicals to react with HO₂, even at the relatively low HO₂ concentrations present. At high NO_x, the RO₂ + NO reactions dominates everything including the RO₂ + HO₂ reaction and very few to no ROOH products are formed.

5 Conclusions

Here we present a model that represents peroxy radical chemistry semi-explicitly and maps the products of that chemistry onto the 2D-VBS. We investigate the dependence of the product yields on temperature, NO_x, and the energy barrier to ~~auto-oxidation~~autoxidation. Ultimately both HOM and dimers are suppressed under conditions when ~~auto-oxidation~~autoxidation is suppressed via the competition with radical termination processes. Competition with bimolecular termination processes is enhanced when the RO₂ lifetime with respect to bimolecular radical termination is shortened (higher radical concentrations) or when ~~auto-oxidation~~autoxidation is slower (higher energy barrier). Therefore HOM and dimer production is highest under high temperature, low NO_x conditions and if we assume a lower energy barrier to ~~auto-oxidation~~autoxidation. These simulations were conducted assuming relatively fast dimerization rate constants. Therefore should some or all peroxy radicals dimerize slower, another important competition, that is not discussed at length here due to its relatively low impact, the RO₂ + HO₂ reaction, could be much more important.

Overall, our simulation results are consistent with emerging experimental observations and strongly suggest that HOM formation will be strongly temperature dependent under atmospheric conditions, as well as highly sensitive to NO. The new “radical” VBS allows us to explicitly simulate the RO₂ termination without making ad-hoc assumptions about “high” or “low”

NO conditions and also enables general consideration of RO₂ termination chemistry, including cross reactions among RO₂ derived from many hydrocarbon precursors. It is thus well suited to describe these rich chemical systems.

Author contributions. MS conducted the model runs and wrote the paper; NMD designed the study, advised research progress, and commented extensively on the paper drafts.

5 *Competing interests.* The authors declare that they have no conflict of interest.

Acknowledgements. This work was supported by grant AGS 1801897 from the U. S. National Science Foundation.

References

- Atkinson, R.: Gas phase tropospheric chemistry of organic compounds, *Journal of Physical and Chemical Reference Data*, 26, 215–290, <https://doi.org/10.1063/1.556012>, 1997.
- Atkinson, R., Baulch, D. L., Cox, R. A., Crowley, J. N., Hampson, R. F., Hynes, R. G., Jenkin, M. E., Rossi, M. J., Troe, J., and Wallington, T. J.: Evaluated kinetic and photochemical data for atmospheric chemistry: Volume IV - gas phase reactions of organic halogen species, *Atmospheric Chemistry and Physics*, 8, 4141–4496, 2008.
- Berndt, T., Scholz, W., Mentler, B., Fischer, L., Herrmann, H., Kulmala, M., and Hansel, A.: Accretion Product Formation from Self- and Cross-Reactions of RO₂ Radicals in the Atmosphere, *Angewandte Chemie International Edition*, 57, 3820–3824, <https://doi.org/10.1002/anie.201710989>, <https://onlinelibrary.wiley.com/doi/abs/10.1002/anie.201710989>, 2018.
- Bianchi, F., Kurtén, T., Riva, M., Mohr, C., Rissanen, M., Pontus, R., Berndt, T., Crounse, J., Wennberg, P., Mentel, T. F., Wildt, J., Junninen, H., Jokinen, T., Kulmala, M., Worsnop, D., Thornton, J., Donahue, N. M., Kjaergaard, H. G., and Ehn, M.: Highly-oxygenated organic molecules (HOM) from gas-phase autoxidation of organic peroxy radicals: A key contributor to atmospheric aerosol, *Chemical Reviews*, 119, 3472–3509, <https://doi.org/10.1021/acs.chemrev.8b00395>, <https://pubs.acs.org/doi/10.1021/acs.chemrev.8b00395>, 2019.
- Chuang, W. K. and Donahue, N. M.: A 2-Dimensional Volatility Basis Set – Part 3: Prognostic modeling and NO_x dependence, *Atmospheric Chemistry and Physics*, 16, 123–134, <https://doi.org/10.5194/acp-16-123-2016>, <http://www.atmos-chem-phys.net/16/123/2016/>, 2016.
- Crounse, J. D., Nielsen, L. B., Jørgensen, S., Kjaergaard, H. G., and Wennberg, P. O.: Autoxidation of Organic Compounds in the Atmosphere, *The Journal of Physical Chemistry Letters*, 4, 3513–3520, <https://doi.org/10.1021/jz4019207>, <http://pubs.acs.org/doi/abs/10.1021/jz4019207>, 2013.
- Donahue, N. M. and Prinn, R. G.: Nonmethane Hydrocarbon Chemistry in the Remote Marine Boundary Layer, *Journal of Geophysical Research Atmospheres*, 95, 18 387–18 411, <http://www.agu.org/pubs/crossref/1990/JD095iD11p18387.shtml>, 1990.
- Donahue, N. M., Huff Hartz, K. E., Chuong, B., Presto, A. A., Stanier, C. O., Rosenørn, T., Robinson, A. L., and Pandis, S. N.: Critical Factors Determining the Variation in SOA Yields from Terpene Ozonolysis: A Combined Experimental and Computational Study, *Faraday Discussions*, 130, 295–309, <http://www.rsc.org/Publishing/Journals/FD/article.asp?doi=b417369d>, 2005.
- Donahue, N. M., Robinson, A. L., Stanier, C. O., and Pandis, S. N.: Coupled Partitioning, Dilution, and Chemical Aging of Semivolatile Organics, *Environmental Science & Technology*, 40, 2635 – 2643, <https://doi.org/10.1021/es052297c>, <http://dx.doi.org/10.1021/es052297c>, 2006.
- Donahue, N. M., Epstein, S. A., Pandis, S. N., and Robinson, A. L.: A Two-Dimensional Volatility Basis Set: 1. Organic Mixing Thermodynamics, *Atmospheric Chemistry and Physics*, 11, 3303–3318, <https://doi.org/10.5194/acp-11-3303-2011>, <http://www.atmos-chem-phys.net/11/3303/2011/>, 2011.
- Donahue, N. M., Henry, K. M., Mentel, T. F., Scharr, A. K., Spindler, C., Bohn, B., Brauers, T., Dorn, H. P., Fuchs, H., Tillmann, R., Wahner, A., Saathoff, H., Naumann, K. H., Möhler, O., Leisner, T., Müller, L., Reinnig, M.-C., Hoffmann, T., Salow, K., Hallquist, M., Frosch, M., Bilde, M., Tritscher, T., Barmet, P., Praplan, A. P., DeCarlo, P. F., Dommen, J., Prévôt, A. S. H., and Baltensperger, U.: Aging of Biogenic Secondary Organic Aerosol via Gas-Phase OH Radical Reactions, *Proceedings of the National Academy of Sciences*, 109, 13 503–13 508, <https://doi.org/10.1073/pnas.1115186109>, <http://www.pnas.org/content/109/34/13503.abstract>, 2012a.
- Donahue, N. M., Kroll, J. H., Robinson, A. L., and Pandis, S. N.: A two-dimensional volatility basis set - Part 2: Diagnostics of organic-aerosol evolution, *Atmospheric Chemistry and Physics*, 12, 615–634, <https://doi.org/10.5194/acp-12-615-2012>, <http://www.atmos-chem-phys.net/12/615/2012/>, 2012b.

- Donahue, N. M., Chuang, W. K., Epstein, S. A., Kroll, J. H., Worsnop, D. R., Robinson, A. L., Adams, P. J., and Pandis, S. N.: Why Do Organic Aerosols Exist? Understanding Aerosol Lifetimes using the Two-Dimensional Volatility Basis Set, *Environmental Chemistry*, 10, 151–157, <https://doi.org/10.1071/EN13022>, <http://dx.doi.org/10.1071/EN13022>, 2013.
- 5 Ehn, M., Thornton, J. A., Kleist, E., Sipila, M., Junninen, H., Pullinen, I., Springer, M., Rubach, F., Tillmann, R., Lee, B., Lopez-Hilfiker, F., Andres, S., Acir, I.-H., Rissanen, M., Jokinen, T., Schobesberger, S., Kangasluoma, J., Kontkanen, J., Nieminen, T., Kurten, T., Nielsen, L. B., Jorgensen, S., Kjaergaard, H. G., Canagaratna, M., Maso, M. D., Berndt, T., Petaja, T., Wahner, A., Kerminen, V.-M., Kulmala, M., Worsnop, D. R., Wildt, J., and Mentel, T. F.: A large source of low-volatility secondary organic aerosol, *Nature*, 506, 476–479, 2014.
- 10 Frege, C., Ortega, I. K., Rissanen, M. P., Praplan, A. P., Steiner, G., Heinritzi, M., Ahonen, L., Amorim, A., Bernhammer, A.-K., Bianchi, F., Brilke, S., Breitenlechner, M., Dada, L., Dias, A., Duplissy, J., Ehrhart, S., El-Haddad, I., Fischer, L., Fuchs, C., Garmash, O., Gonin, M., Hansel, A., Hoyle, C. R., Jokinen, T., Junninen, H., Kirkby, J., Kürten, A., Lehtipalo, K., Leiminger, M., Mauldin, R. L., Molteni, U., Nichman, L., Petäjä, T., Sarnela, N., Schobesberger, S., Simon, M., Sipilä, M., Stolzenburg, D., Tomé, A., Vogel, A. L., Wagner, A. C., Wagner, R., Xiao, M., Yan, C., Ye, P., Curtius, J., Donahue, N. M., Flagan, R. C., Kulmala, M., Worsnop, D. R., Winkler, P. M., Dommen, J., and Baltensperger, U.: Influence of temperature on the molecular composition of ions and charged clusters during pure biogenic nucleation, *Atmospheric Chemistry and Physics*, 18, 65–79, <https://doi.org/10.5194/acp-18-65-2018>, <https://www.atmos-chem-phys.net/18/65/2018/>,
15 2018.
- Fry, J. L., Draper, D. C., Barsanti, K. C., Smith, J. N., Ortega, J., Winkler, P. M., Lawler, M. J., Brown, S. S., Edwards, P. M., Cohen, R. C., and Lee, L.: Secondary Organic Aerosol Formation and Organic Nitrate Yield from NO₃ Oxidation of Biogenic Hydrocarbons, *Environmental Science & Technology*, 48, 11 944–11 953, <https://doi.org/10.1021/es502204x>, <https://doi.org/10.1021/es502204x>, PMID: 25229208, 2014.
- 20 Henry, K. M. and Donahue, N. M.: Effect of the OH radical scavenger hydrogen peroxide on secondary organic aerosol formation from α -pinene ozonolysis, *Aerosol Science and Technology*, 45, 686–690, <https://doi.org/10.1080/02786826.2011.552926>, <http://www.informaworld.com/smpp/content~db=all~content=a933399706~frm=titlelink>, 2011.
- Jimenez, J. L., Canagaratna, M. R., Donahue, N. M., Prévôt, A. S. H., Zhang, Q., Kroll, J. H., DeCarlo, P. F., Allan, J., Coe, H., Ng, N. L., Aiken, A. C., Docherty, K. D., Ulbrich, I. M., Grieshop, A. P., Robinson, A. L., Duplissy, J., Smith, J. D., Wilson, K. R., Lanz, V. A.,
25 Hueglin, C., Sun, Y. L., Laaksonen, A., Raatikainen, T., Rautiainen, J., Vaattovaara, P., Ehn, M., Kulmala, M., Tomlinson, J. M., Collins, D. R., Cubison, M. J., Dunlea, E. J., Huffman, J. A., Onasch, T. B., Alfarra, M. R., Williams, P. I., Bower, K., Kondo, Y., Schneider, J., Drewnick, F., Borrmann, S., Weimer, S., Demerjian, K., Salcedo, D., Cottrell, L., Griffin, R., Takami, A., Miyoshi, T., Hatakeyama, S., Shimono, A., Sun, J. Y., Zhang, Y. M., Dzepina, K., Kimmel, J. R., Sueper, D., Jayne, J. T., Herndon, S. C., Trimborn, A. M., Williams, L. R., Wood, E. C., Kolb, C. E., Baltensperger, U., and Worsnop, D. R.: Evolution of Organic Aerosols in the Atmosphere, *Science*, 326,
30 1525–1529, <https://doi.org/10.1126/science.1180353>, <http://www.sciencemag.org/cgi/content/abstract/326/5959/1525>, 2009.
- Kirkby, J., Duplissy, J., Sengupta, K., Frege, C., Gordon, H., Williamson, C., Heinritzi, M., Simon, M., Yan, C., Almeida, J., Tröstl, J., Nieminen, T., Ortega, I. K., Wagner, R., Adamov, A., Amorim, A., Bernhammer, A.-K., Bianchi, F., Breitenlechner, M., Brilke, S., Chen, X., Craven, J., Dias, A., Ehrhart, S., Flagan, R. C., Franchin, A., Fuchs, C., Guida, R., Hakala, J., Hoyle, C. R., Jokinen, T., Junninen, H., Kangasluoma, J., Kim, J., Krapf, M., Kürten, A., Laaksonen, A., Lehtipalo, K., Makhmutov, V., Mathot, S., Molteni, U., Onnela, A.,
35 Peräkylä, O., Piel, F., Petäjä, T., Praplan, A. P., Pringle, K., Rap, A., Richards, N. A., Riipinen, I., Rissanen, M. P., Rondo, L., Sarnela, N., Schobesberger, S., Scott, C. E., Seinfeld, J. H., Sipilä, M., Steiner, G., Stozhkov, Y., Stratmann, F., Tomé, A., Virtanen, A., Vogel, A. L., Wagner, A., Wagner, P. E., Weingartner, E., Wimmer, D., Winkler, P. M., Ye, P., Zhang, X., Hansel, A., Dommen, J., Donahue, N. M.,

- Worsnop, D. R., Baltensperger, U., Kulmala, M., Carslaw, K. S., and Curtius, J.: Ion-induced nucleation of pure biogenic particles, *Nature*, 530, 521–526, <https://doi.org/10.1038/nature17953>, <http://dx.doi.org/10.1038/nature17953>, 2016.
- Kurtén, T., Tiusanen, K., Roldin, P., Rissanen, M., Luy, J.-N., and Donahue, N. M.: Saturation Vapor Pressures of α -pinene Autoxidation Products May Be Severely Underpredicted by Group Contribution Methods, *Journal of Physical Chemistry A*, 120, 2569–2582, <https://doi.org/10.1021/acs.jpca.6b02196>, <http://dx.doi.org/10.1021/acs.jpca.6b02196>, 2016.
- Lee, R., Gryn'ova, G., Ingold, K. U., and Coote, M. L.: Why are sec-alkylperoxyl bimolecular self-reactions orders of magnitude faster than the analogous reactions of tert-alkylperoxyls? The unanticipated role of CH hydrogen bond donation, *Physical Chemistry Chemical Physics*, 18, 23 673–23 679, <https://doi.org/10.1039/C6CP04670C>, <http://dx.doi.org/10.1039/C6CP04670C>, 2016.
- Lehtipalo, K., Yan, C., Dada, L., Bianchi, F., Xiao, M., Wagner, R., Stolzenburg, D., Ahonen, L. R., Amorim, A., Baccarini, A., Bauer, P. S., Baumgartner, B., Bergen, A., Bernhammer, A.-K., Breitenlechner, M., Brilke, S., Buckholz, A., Mazon, S. B., Chen, D., Chen, X., Dias, A., Dommen, J., Draper, D. C., Duplissy, J., Ehn, M., Finkenzeller, H., Fisher, L., Frege, C., Fuchs, C., Garmash, O., Gordon, H., Hakala, J., He, X. C., Heikkinen, L., Heinrizi, M., Helm, J. C., Hofbauer, V., Hoyle, C. R., Jokinen, T., Kangasluoma, J., Kerminen, V.-M., Kim, C., Kirkby, J., Kontkanen, J., Kürten, A., Lawler, M. J., Mai, H., Mathot, S., Mauldin III, R. L., Molteni, U., Nichman, L., Nie, W., Nieminen, T., Ojdanic, A., Onnela, A., Passananti, M., Petäjä, T., Piel, F., Pospisilova, V., Quéléver, L. L. J., Rissanen, M. P., Rose, C., Sarnela, N., Schallhart, S., Sengupta, K., Simon, M., Tauber, C., Tomé, A., Tröstl, J., Väisänen, O., Voge, A. L., Volkamer, R., Wagner, A. C., Wang, M., Weitz, L., Wimmer, D., Ye, P., Ylisirniö, A., Zha, Q., Carslaw, K., Curtius, J., Donahue, N., Flagan, R. C., Hansel, A., Riipinen, I., Virtanen, A., Winkler, P. M., Baltensperger, U., Kulmala, M., and Worsnop, D. R.: Multi-component new particle formation from sulfuric acid, ammonia and biogenic vapors, *Science Advances*, 4, 1–9, <https://doi.org/10.1126/sciadv.aau5363>, <http://advances.sciencemag.org/content/4/12/eaau5363>, 2018.
- Lim, Y. B. and Ziemann, P. J.: Effects of Molecular Structure on Aerosol Yields from OH Radical-Initiated Reactions of Linear, Branched, and Cyclic Alkanes in the Presence of NO_x, *Environmental Science & Technology*, 43, 2328–2334, 2009.
- Madronich, S. and Calvert, J. G.: Atmospheric Chemistry of small organic peroxy radicals, *Journal of Geophysical Research Atmospheres*, 95, 5697, 1990.
- Mihelcic, D., Holland, F., Hofzumahaus, A., Hoppe, L., Konrad, S., Müsgen, P., Pätz, H.-W., Schäfer, H.-J., Schmitz, T., Volz-Thomas, A., Bächmann, K., Schlomski, S., Platt, U., Geyer, A., Alicke, B., and Moortgat, G.: Peroxy radicals during BERLIOZ at Pabstthum: Measurements, radical budgets and ozone production, *Journal of Geophysical Research: Atmospheres*, 108, <https://doi.org/10.1029/2001JD001014>, <https://agupubs.onlinelibrary.wiley.com/doi/abs/10.1029/2001JD001014>, 2003.
- Molteni, U., Simon, M., Heinrizi, M., Hoyle, C. R., Bernhammer, A.-K., Bianchi, F., Breitenlechner, M., Brilke, S., Dias, A., Duplissy, J., Frege, C., Gordon, H., Heyn, C., Jokinen, T., Kürten, A., Lehtipalo, K., Makhmutov, V., Petäjä, T., Pieber, S. M., Praplan, A. P., Schobesberger, S., Steiner, G., Stozhkov, Y., Tomé, A., Tröstl, J., Wagner, A. C., Wagner, R., Williamson, C., Yan, C., Baltensperger, U., Curtius, J., Donahue, N. M., Hansel, A., Kirkby, J., Kulmala, M., Worsnop, D. R., and Dommen, J.: Formation of highly-oxygenated organic molecules from α -pinene ozonolysis: chemical characteristics, mechanism and kinetic model development, *Earth and Space Chemistry*, 3, in press, 2019.
- Ng, N. L., Brown, S. S., Archibald, A. T., Atlas, E., Cohen, R. C., Crowley, J. N., Day, D. A., Donahue, N. M., Fry, J. L., Fuchs, H., Griffin, R. J., Guzman, M. I., Herrmann, H., Hodzic, A., Iinuma, Y., Jimenez, J. L., Kiendler-Scharr, A., Lee, B. H., Luecken, D. J., Mao, J., McLaren, R., Mutzel, A., Osthoff, H. D., Ouyang, B., Picquet-Varrault, B., Platt, U., Pye, H. O. T., Rudich, Y., Schwantes, R. H., Shiraiwa, M., Stutz, J., Thornton, J. A., Tilgner, A., Williams, B. J., and Zaveri, R. A.: Nitrate radicals and biogenic volatile organic compounds:

- oxidation, mechanisms, and organic aerosol, *Atmospheric Chemistry and Physics*, 17, 2103–2162, <https://doi.org/10.5194/acp-17-2103-2017>, <http://www.atmos-chem-phys.net/17/2103/2017/>, 2017.
- Pankow, J. F. and Asher, W. E.: SIMPOL.1: A simple group contribution method for predicting vapor pressures and enthalpies of vaporization of multifunctional organic compounds, *Atmospheric Chemistry and Physics*, 7, 11 839–11 894, <http://www.atmos-chem-phys-discuss.net/7/11839/2007/>, 2007.
- 5 Presto, A. A. and Donahue, N. M.: Ozonolysis Fragment Quenching by Nitrate Formation: The Pressure Dependence of Prompt OH Radical Formation, *Journal of Physical Chemistry A*, 108, 9096–9104, <http://pubs.acs.org/doi/abs/10.1021/jp047162s>, 2004.
- Presto, A. A. and Donahue, N. M.: Investigation of α -pinene + ozone Secondary Organic Aerosol Formation at Low Total Aerosol Mass, *Environmental Science & Technology*, 40, 3536–3543, <https://doi.org/10.1021/es052203z>, <http://dx.doi.org/10.1021/es052203z>, 2006.
- 10 Rissanen, M. P., Kurtén, T., Sipilä, M., Thornton, J. A., Kangasluoma, J., Sarnela, N., Junninen, H., Jørgensen, S., Schallhart, S., Kajos, M. K., Taipale, R., Springer, M., Mentel, T. F., Ruuskanen, T., Petäjä, T., Worsnop, D. R., Kjaergaard, H. G., and Ehn, M.: The Formation of Highly Oxidized Multifunctional Products in the Ozonolysis of Cyclohexene, *Journal of the American Chemical Society*, 136, 15 596–15 606, <https://doi.org/10.1021/ja507146s>, <http://dx.doi.org/10.1021/ja507146s>, PMID: 25283472, 2014.
- Schobesberger, S., Junninen, H., Bianchi, F., Lönn, G., Ehn, M., Lehtipalo, K., Dommen, J., Ehrhart, S., Ortega, I. K., Franchin, A., Nieminen, T., Riccobono, F., Hutterli, M., Duplissy, J., Almeida, J., Amorim, A., Breitenlechner, M., Downard, A. J., Dunne, E. M., Flagan, R. C., Kajos, M., Keskinen, H., Kirkby, J., Kupc, A., Kürten, A., Kurtén, T., Laaksonen, A., Mathot, S., Onnela, A., Rondo, A. P. P. L., Santos, F. D., Schallhart, S., Schnitzhofer, R., Sipilä, M., Tomé, A., Tsagkogeorgas, G., Vehkamäki, H., Wimmer, D., Baltensperger, U., Carslaw, K. S., Curtius, J., Hansel, A., Petäjä, T., Kulmala, M., Donahue, N. M., and Worsnop, D. R.: Molecular understanding of atmospheric particle formation from sulfuric acid and large oxidized organic molecules, *Proceedings of the National Academy of Sciences*, 110, 17 223–17 228, <https://doi.org/10.1073/pnas.1306973110>, <http://www.pnas.org/cgi/doi/10.1073/pnas.1306973110>, 2013.
- 15 Stolzenburg, D., Fischer, L., Vogel, A. L., Heinritzi, M., Schervish, M., Simon, M., Wagner, A. C., Dada, L., Ahonen, L. R., Amorim, A., Baccarini, A., Bauer, P. S., Baumgartner, B., Bergen, A., Bianchi, F., Breitenlechner, M., Brilke, S., Buenrostro Mazon, S., Chen, D., Dias, A., Draper, D. C., Duplissy, J., El Haddad, I., Finkenzeller, H., Frege, C., Fuchs, C., Garmash, O., Gordon, H., He, X., Helm, J., Hofbauer, V., Hoyle, C. R., Kim, C., Kirkby, J., Kontkanen, J., Kürten, A., Lampilahti, J., Lawler, M., Lehtipalo, K., Leiminger, M., Mai, H., Mathot, S., Mentler, B., Molteni, U., Nie, W., Nieminen, T., Nowak, J. B., Ojdanic, A., Onnela, A., Passananti, M., Petäjä, T., Quéléver, L. L. J., Rissanen, M. P., Sarnela, N., Schallhart, S., Tauber, C., Tomé, A., Wagner, R., Wang, M., Weitz, L., Wimmer, D., Xiao, M., Yan, C., Ye, P., Zha, Q., Baltensperger, U., Curtius, J., Dommen, J., Flagan, R. C., Kulmala, M., Smith, J. N., Worsnop, D. R., Hansel, A., Donahue, N. M., and Winkler, P. M.: Rapid growth of organic aerosol nanoparticles over a wide tropospheric temperature range, *Proceedings of the National Academy of Sciences*, 115, 9122–9127, <https://doi.org/10.1073/pnas.1807604115>, <http://www.pnas.org/content/115/37/9122>, 2018.
- 20 Tan, Z., Rohrer, F., Lu, K., Ma, X., Bohn, B., Broch, S., Dong, H., Fuchs, H., Gkatzelis, G. I., Hofzumahaus, A., Holland, F., Li, X., Liu, Y., Liu, Y., Novelli, A., Shao, M., Wang, H., Wu, Y., Zeng, L., Hu, M., Kiendler-Scharr, A., Wahner, A., and Zhang, Y.: Wintertime photochemistry in Beijing: observations of RO₂ radical concentrations in the North China Plain during the BEST-ONE campaign, *Atmospheric Chemistry and Physics*, 18, 12 391–12 411, <https://doi.org/10.5194/acp-18-12391-2018>, <https://www.atmos-chem-phys.net/18/12391/2018/>, 2018.
- 25 Tröstl, J., Chuang, W. K., Heinritzi, M., Yan, C., Molteni, U., Ahlm, L., Frege, C., Bianchi, F., Wagner, R., Simon, M., Lehtipalo, K., Williamson, C., Craven, J. S., Duplissy, J., Adamov, A., Almeida, J., Bernhammer, A.-K., Breitenlechner, M., Brilke, S., Dias, A., Ehrhart, S., Flagan, R. C., Franchin, A., Fuchs, C., Gordon, H., Guida, R., Gysel, M., Hansel, A., Hoyle, C. R., Jokinen, T., Junninen, H., Kangasluoma, J., Keskinen, H., Kim, J., Krapf, M., Kürten, A., Laaksonen, A., Lawler, M., Leiminger, M., Mathot, S., Möhler, O., Nieminen,
- 30

- T., Onnela, A., Petäjä, T., Piel, F. M., Miettinen, P., Rissanen, M. P., Rondo, L., Sarnela, N., Schobesberger, S., Sengupta, K., Sipilä, M., Smith, J. N., Steiner, G., Tomè, A., Virtanen, A., Wagner, A. C., Weingartner, E., Wimmer, D., Winkler, P. M., Ye, P., Carslaw, K. S., Curtius, J., Dommen, J., Kirkby, J., Kulmala, M., Riipinen, I., Worsnop, D. R., Donahue, N. M., and Baltensperger, U.: The role of low-volatility organic compounds in initial particle growth in the atmosphere, *Nature*, 530, 527–531, <https://doi.org/10.1038/nature18271>,
5 <http://dx.doi.org/10.1038/nature18271>, 2016.
- Tyndall, G. S., Cox, R. A., Granier, C., Lesclaux, R., Moortgat, G. K., Pilling, M. J., Ravishankara, A. R., and Wallington, T. J.: Atmospheric Chemistry of Small Organic Peroxy Radicals, *J. Geophys. Res.*, 106, 12 157, 2001.
- Wallington, T. J., Daugaut, P., and Kurylo, M. J.: Ultraviolet Absorption Cross Sections and Reaction Kinetics and Mechanisms for Peroxy Radicals in the Gas Phase, *Chemical Reviews*, 92, 667–710, 1992.
- 10 Ye, P., Zhao, Y., Chuang, W. K., Robinson, A. L., and Donahue, N. M.: Secondary organic aerosol production from pinanediol, a semi-volatile surrogate for first-generation oxidation products of monoterpenes, *Atmospheric Chemistry and Physics*, 18, 6171–6186, <https://doi.org/10.5194/acp-18-6171-2018>, <https://www.atmos-chem-phys.net/18/6171/2018/>, 2018.
- Zhao, Y., Saleh, R., Saliba, G., Presto, A. A., Gordon, T. D., Drozd, G. T., Goldstein, A. H., Donahue, N. M., and Robinson, A. L.: Reducing secondary organic aerosol formation from gasoline vehicle exhaust, *Proceedings of the National Academy of Sciences*, 114, 6984–6989,
15 <https://doi.org/10.1073/pnas.1620911114>, <http://www.pnas.org/content/114/27/6984.abstract>, 2017.

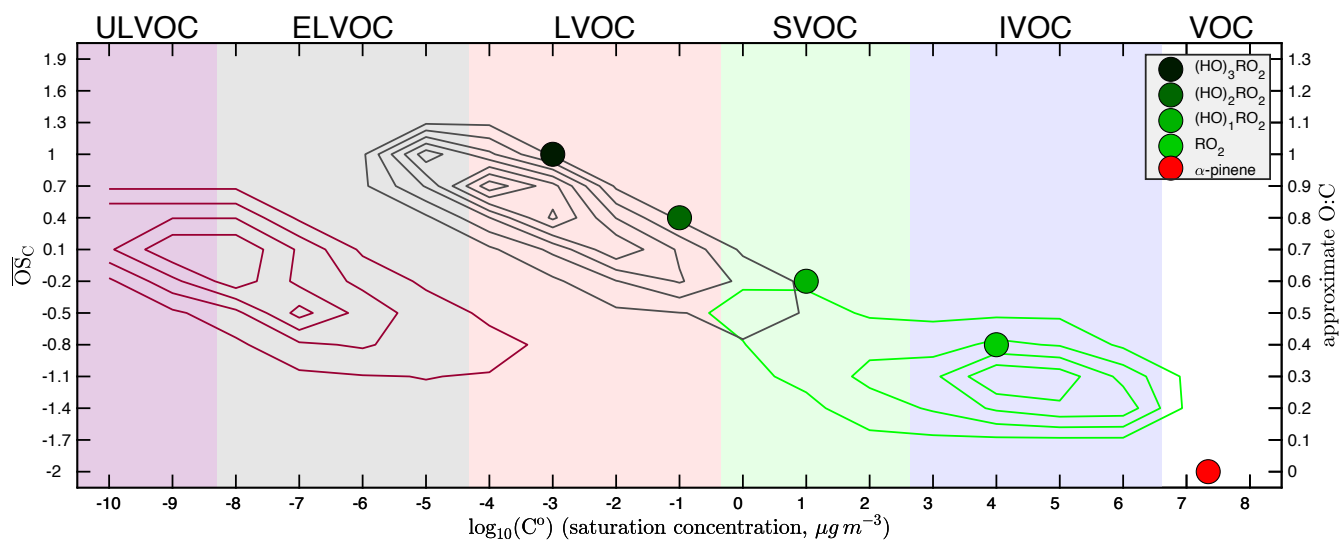


Figure 1. Basic α -pinene oxidation and the two-dimensional volatility basis set (2D-VBS), including explicitly treated peroxy radicals (RO_2). Axes are volatility $\log_{10} C^{\circ}(300\text{K})$ and O:C. Broad colored bands are volatility classes, indicated along the top: ULVOCs are efficient nucleators. α -Pinene (red, lower right) oxidizes to produce a succession of peroxy radicals, first a “traditional” radical (RO_2 , in light green) and then a succession of oxidized RO_2 via auto-oxidation (Ox_nRO_2 , darker shades of green). RO_2 radicals ultimately terminate into molecular products, represented here by contours depending on whether they derive from the traditional RO_2 (green contours), auto-oxidation (C_{10} monomers, gray contours), or Ox_nRO_2 dimerization (C_{20} ROOR, maroon contours).

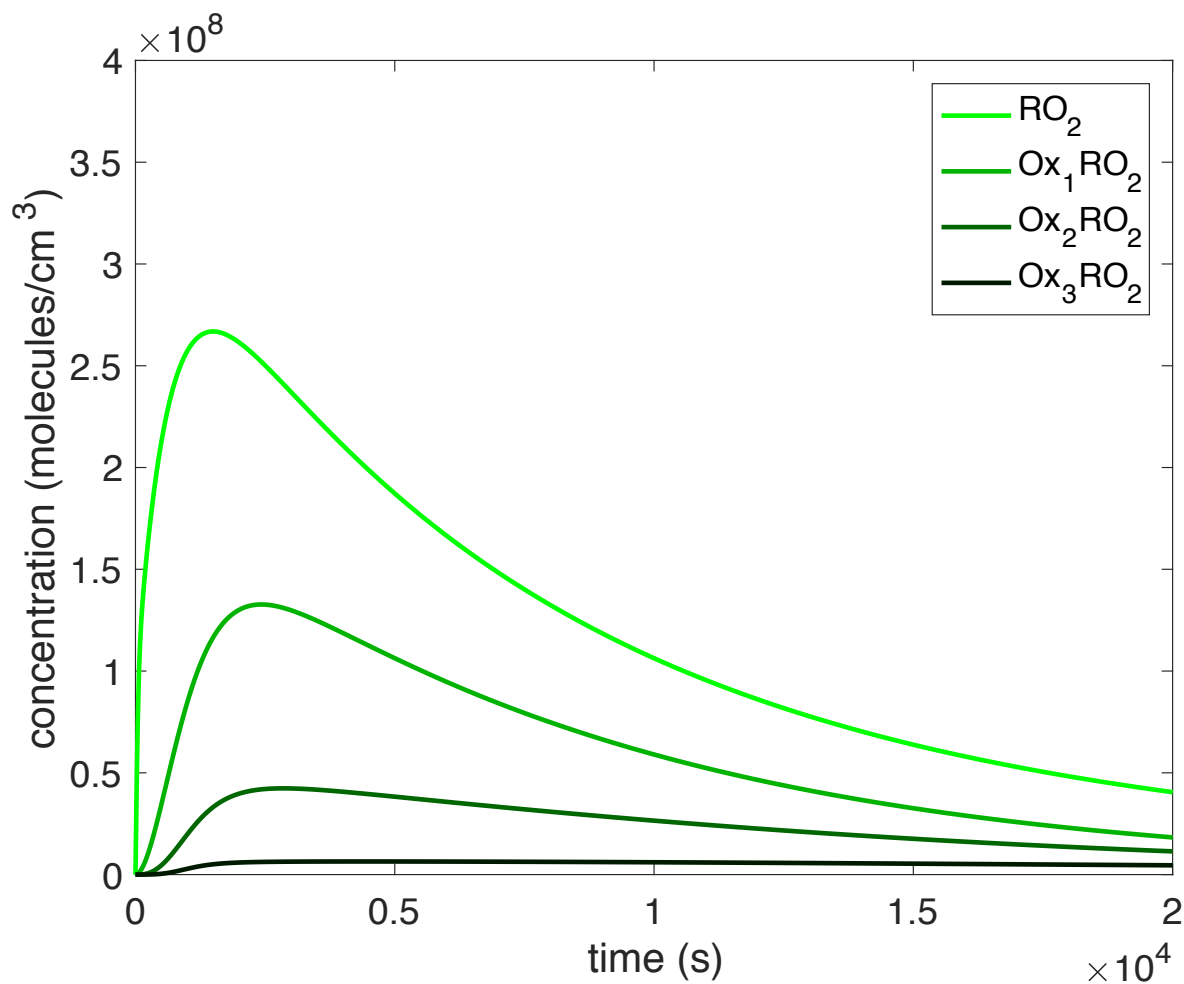


Figure 2. Concentration time series of peroxy radicals (RO_2). The peroxy radical concentrations over the course of a simulation peak early as they are produced via α -pinene oxidation and decrease as ~~they α -pinene decays and the RO_2 react away~~ over the course of the simulation. This simulation is run at 298 K and with no NO_x although the trends are similar across the temperatures and NO_x concentrations investigated here, with the difference being in the absolute concentrations, especially those of the more oxidized peroxy radicals.

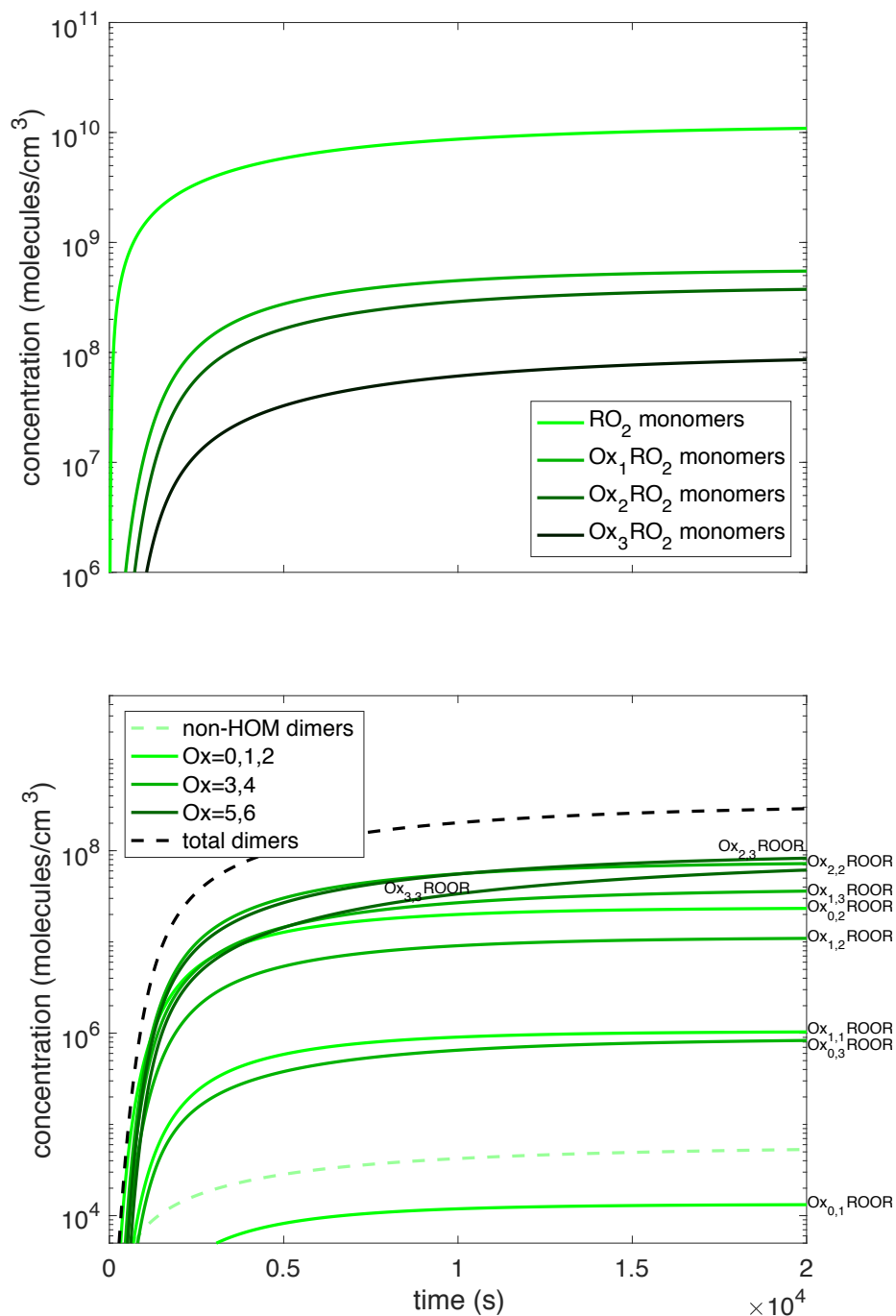


Figure 3. Concentration time series of monomer and dimer products. Ox_{*n*} indicates the number of [auto-oxidation](#) [autooxidation](#) steps. All of these products are formed via peroxy radical chemistry, but the products are still predominantly non-HOM. This trend persists for hydroperoxides and organonitrates when NO_{*x*} is present. The dimers do not follow the same trend of forming more from the less oxidized peroxy radical as the other species do. The dimer plot is colored by the sum of how oxidized the two peroxy radicals that reacted to form the dimer are (i.e. the dimerization of an Ox₁RO₂ and an Ox₂RO₂ would be consider sum of Ox = 3). However, they also do not follow the exact opposite trend. This is due to the branching ratio to dimers being larger for low volatility peroxy radicals, but those peroxy radicals being less common leading to mid-range oxidized peroxy radicals forming [the](#) most dimers.

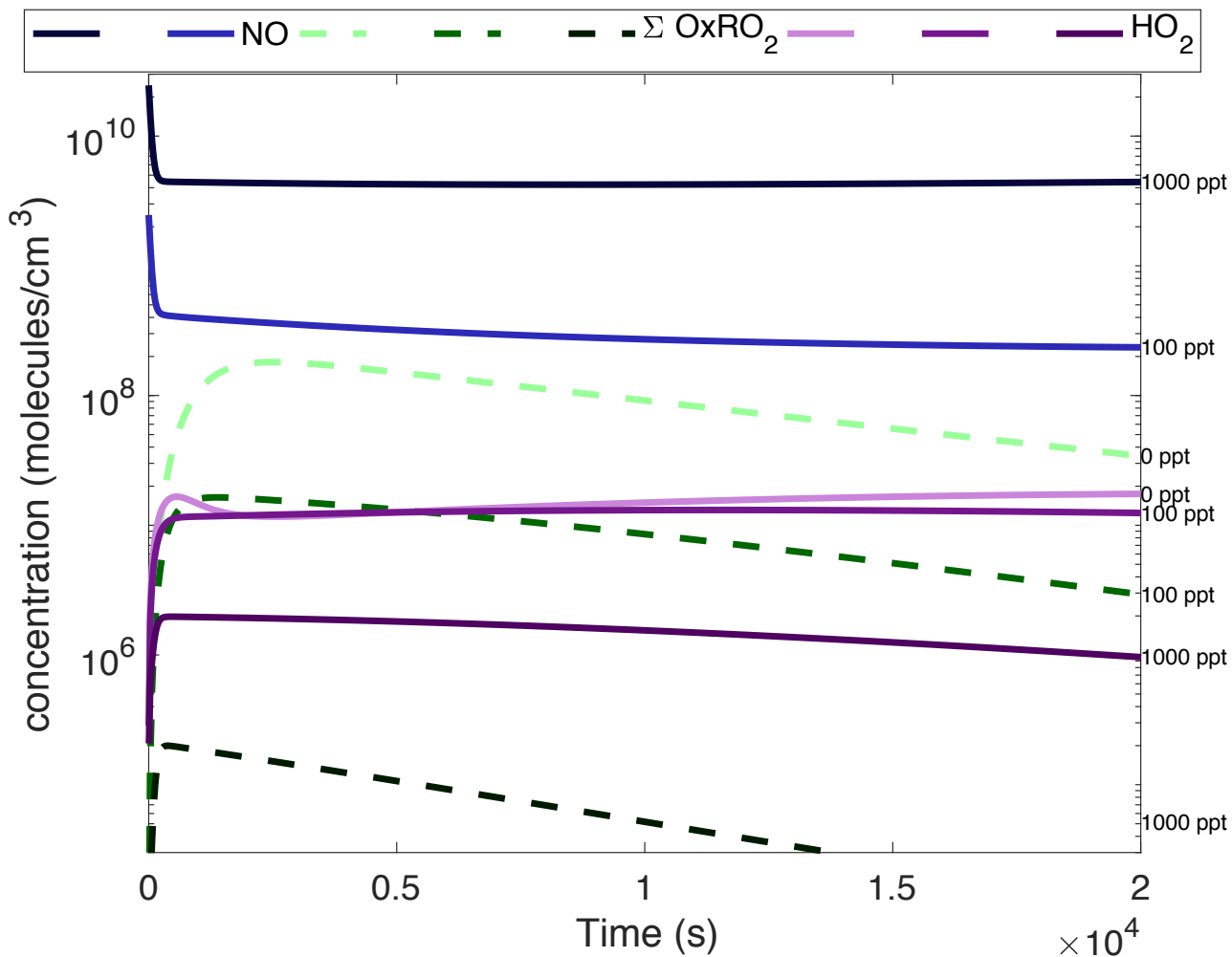


Figure 4. Concentration time series of HO_2 , NO , and oxidized RO_2 at various NO_x levels. [The numbers along the right-hand y-axis refer to the \$\text{NO}_x\$ concentration for each simulation, which is also indicated by the shading of each curve, going from light at low \$\text{NO}_x\$ to dark at high \$\text{NO}_x\$.](#) HO_2 remains reasonably stable near 10^7 molec cm^{-3} (0.3 pptv). NO_x is introduced as NO and drops to a steady state as it reacts with HO_2 and RO_2 to form NO_2 , which in turn photolyzes. By 1000 pptv added NO_x the NO greatly exceeds the HO_2 and somewhat suppresses HO_2 concentrations. The oxidized RO_2 ($\Sigma \text{Ox}_n \text{RO}_2$) reaches a peak just over 10^8 molec cm^{-3} at zero NO_x before gradually decaying [as a function of time](#).

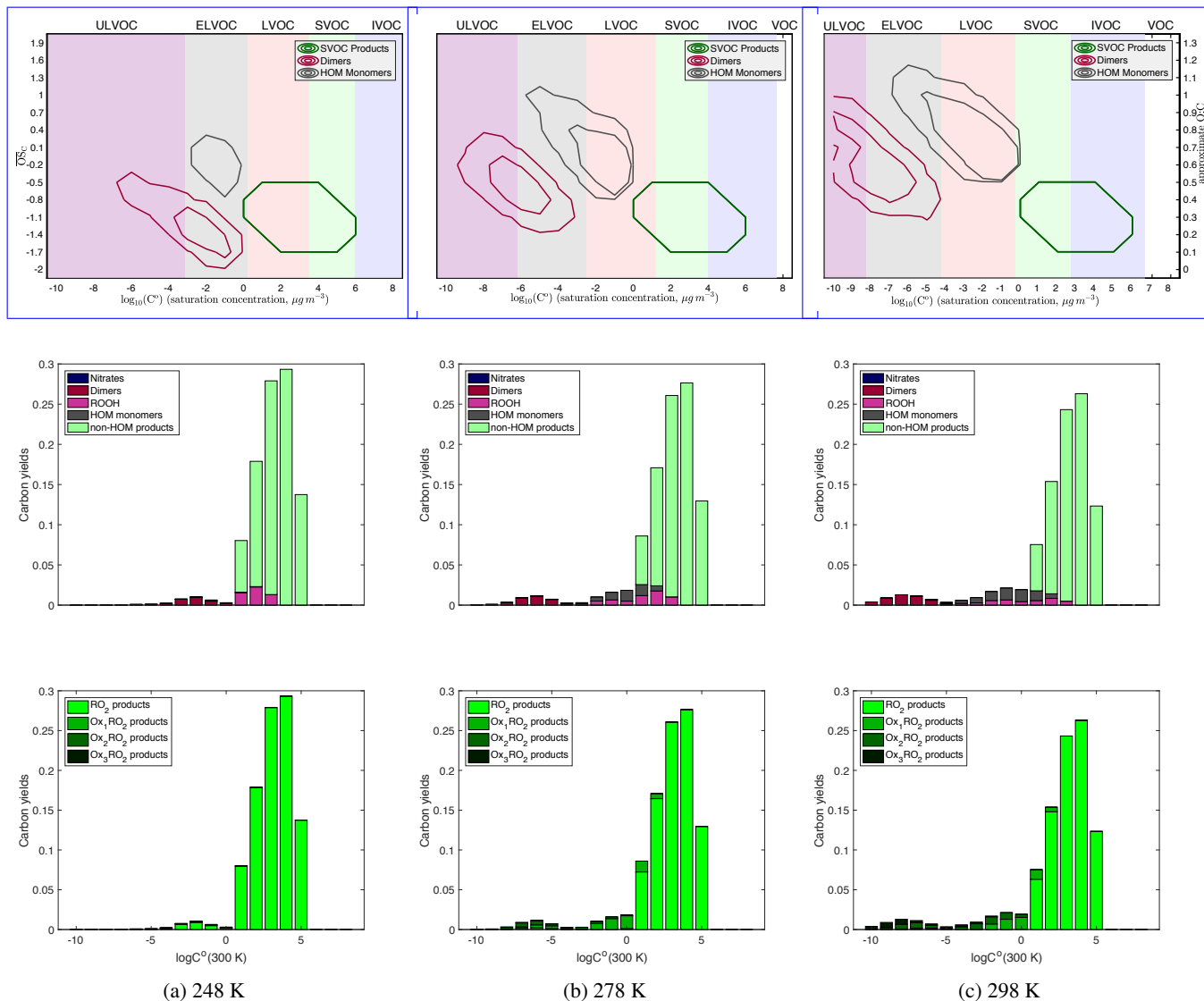


Figure 5. Yields of α -pinene oxidation products without any NO_x present at 248 K, 278K, and 298K. As temperature decreases, in the top, contour plots the dimer products shift to higher volatilities and lower O:C, even to the point where the dimers have approximately the same $C^*(300K/300 K)$ as the monomer products, which is supported by experimental data. In addition, the diversity of both monomer, and dimer products decreases with decreasing temperature. In the middle row of plots, where we color the yields by what type of product they are, we again see that shift of the products to higher volatilities. In addition, we see fewer dimers formed at lower temperatures. **This makes sense based on the hypothesis that when two peroxy radicals react the probability that they formed a dimer is dependent on their volatility, and thus dependent on the extent of auto-oxidation. The dimers formed at the lowest temperature are mostly non-HOM dimers formed from reactions of the initial peroxy radicals, where no auto-oxidation occurred.** It is also of note that the formation of hydroperoxides is not a significant fraction of the yield at any temperature due to the low concentration of HO_2 . The bottom plots, colored by the extent of **auto-oxidation** the products underwent before terminating, show that as we decrease temperature, the extent of **auto-oxidation** that the peroxy radicals undergo decreases. At 248 K, we see almost no products that have undergone any **auto-oxidation**.

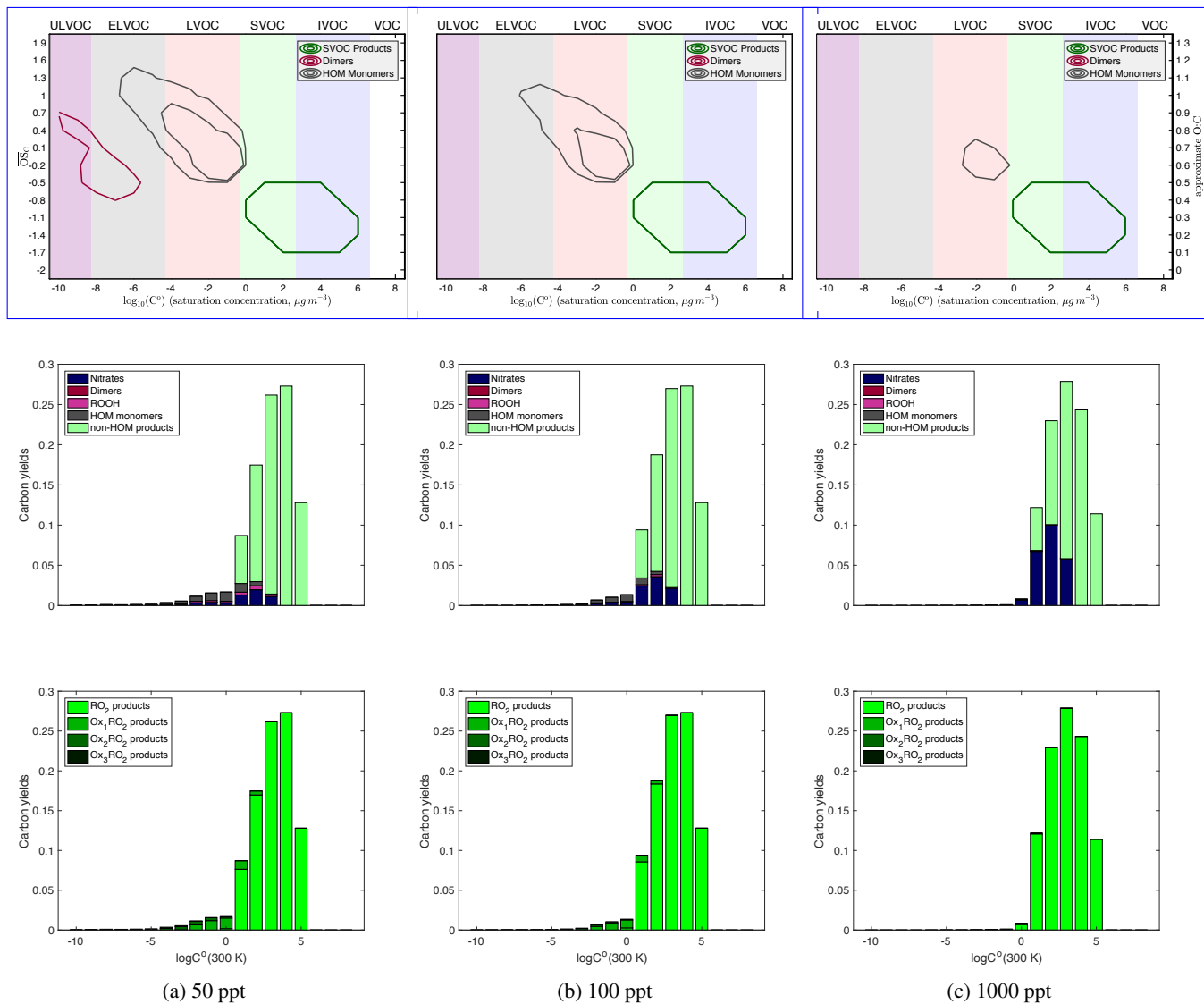


Figure 6. Yields of α -pinene oxidation products ~~without~~ at 298 K with 50, 100, and 1000 ppt of NO_x introduced into the system. There are similar trends seen in the contour plot with an increase in the volatility of both HOM monomer and dimer products as well as a decrease in the diversity of both with increasing NO_x . In the second row of plots, we see an increase in the amount of nitrates formed and the depletion of dimers formed with increasing NO_x . Similarly to the temperature trend, as we increase NO_x the products shift to higher volatilities. However, once we reach a high enough NO_x concentration to produce essentially no dimers, we still see some LVOC products that include nitrates. This is consistent with experimental evidence that NO_x suppresses nucleation, but not necessarily growth. From the last plots, we can clearly see fewer ~~auto-oxidation~~ ~~auto-oxidation~~ products at higher NO_x concentrations with a nearly complete suppression of ~~auto-oxidation~~ ~~auto-oxidation~~ between 500-1000 ppt of NO_x .

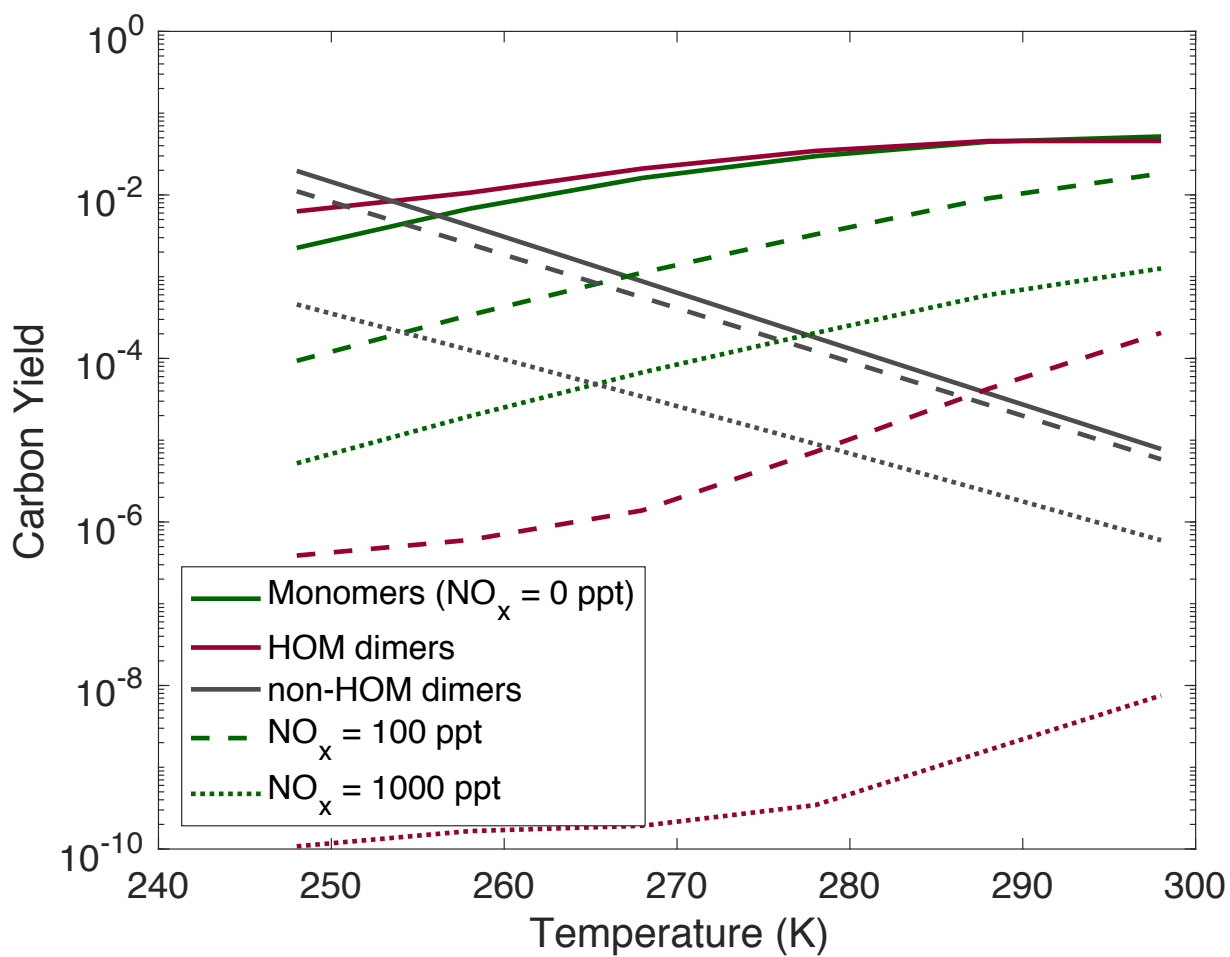


Figure 7. Yields at different temperatures and various NO_x levels: no NO_x present (solid curves), 100 ppt of NO_x present (dashed curves) and 1000 ppt of NO_x present (dotted curves). Very low NO_x concentrations have little effect on HOM yields, however NO_x eventually becomes competitive with HOM-producing pathways and there is a significant reduction in both dimer and HOM monomer yields accompanied by an increase in non-HOM dimers. HOM dimers are more strongly affected by suppression of ~~auto-oxidation~~ autoxidation than HOM monomers.

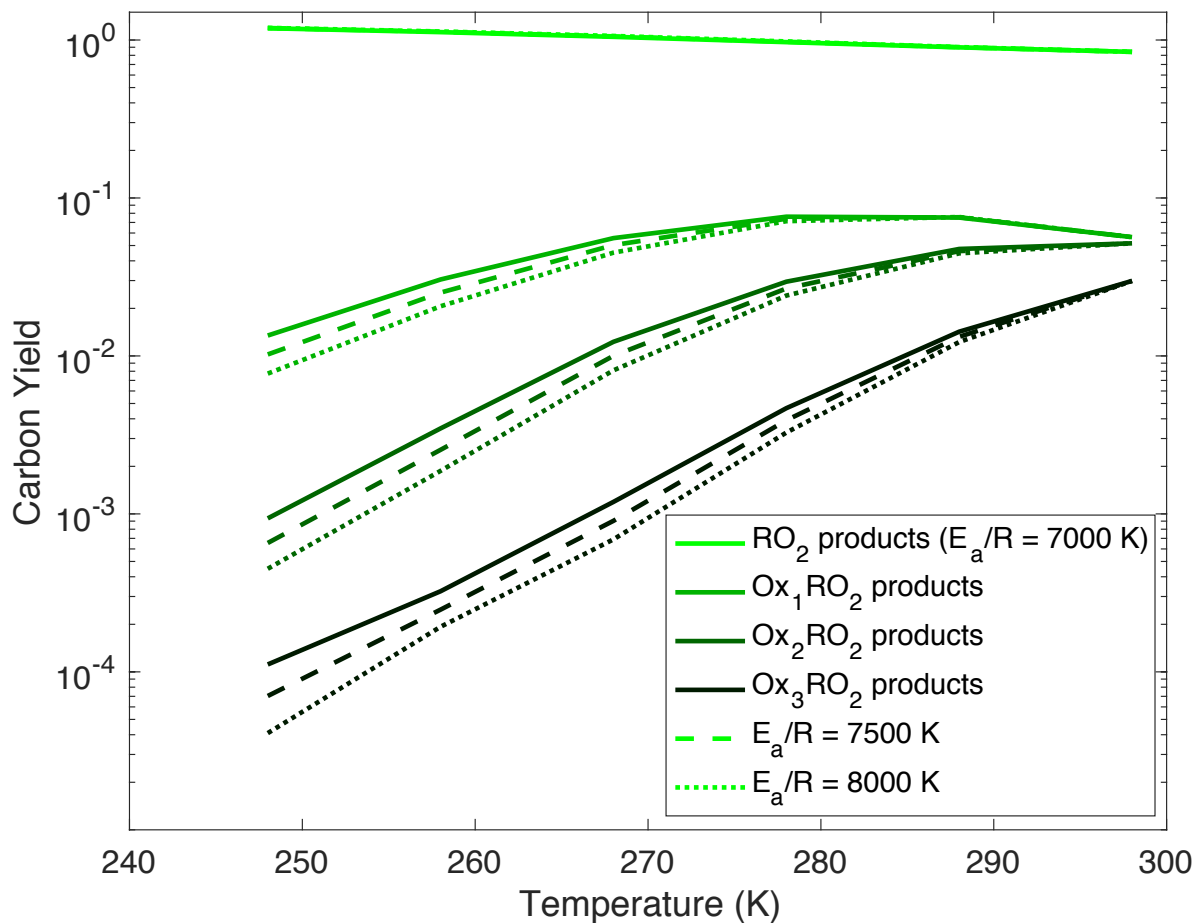


Figure 8. Variation in carbon yields of the OxRO₂s with temperature for different auto-oxidation-~~autoxidation~~ barrier heights. Here the auto-oxidation-~~autoxidation~~ rate coefficient at 298 K is fixed at 0.01 s⁻¹ and we vary the activation energy. The dashed curve shows the results for the rate coefficient in our base-case simulation. The solid curve has a lower activation energy and thus a weaker temperature dependence, while the dotted curve has a higher activation energy and thus a stronger temperature dependence. As expected auto-oxidation-~~autoxidation~~ is suppressed more quickly as temperature drops when the activation energy is higher; this translates to lower HOM yields.

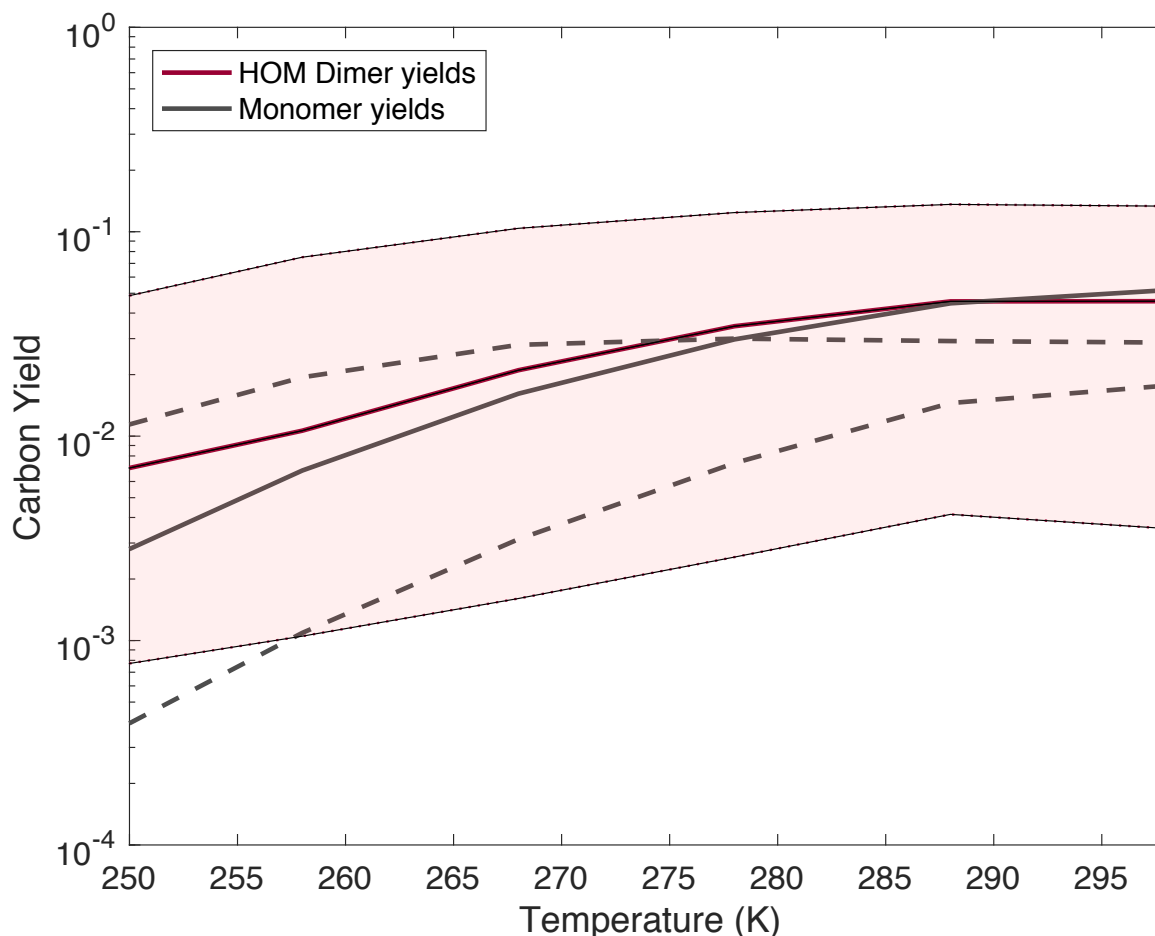


Figure 9. Changes to HOM monomer and dimer yields with an order of magnitude variation in the rate coefficient at 298 K by changing the [auto-oxidation-oxidation](#) A factor. The rate coefficient at temperatures other than 298 K is calculated in the same manner as described above. Almost all of the yields at a particular temperature are increased relative to the traditional case when we assume the rate coefficient at 298 K is higher than the traditional case and the yields decrease at a particular temperature when we assume the rate coefficient is lower than the traditional case. The monomer yields decrease with a faster [auto-oxidation-oxidation](#) rate constant at high temperatures because with more [auto-oxidation-oxidation](#), more association reactions successfully form dimers, thus reducing the monomer yields. Quantitatively, as we vary the rate coefficient of [auto-oxidation-oxidation](#) by an order of magnitude, we are seeing a corresponding increase or decrease in the HOM product also by about an order of magnitude. [The monomer yields are shown in dashed lines and show a more complicated trend with the low barrier monomer yields being higher than the “base-case” yields at lower temperatures, but lower at high temperatures.](#)

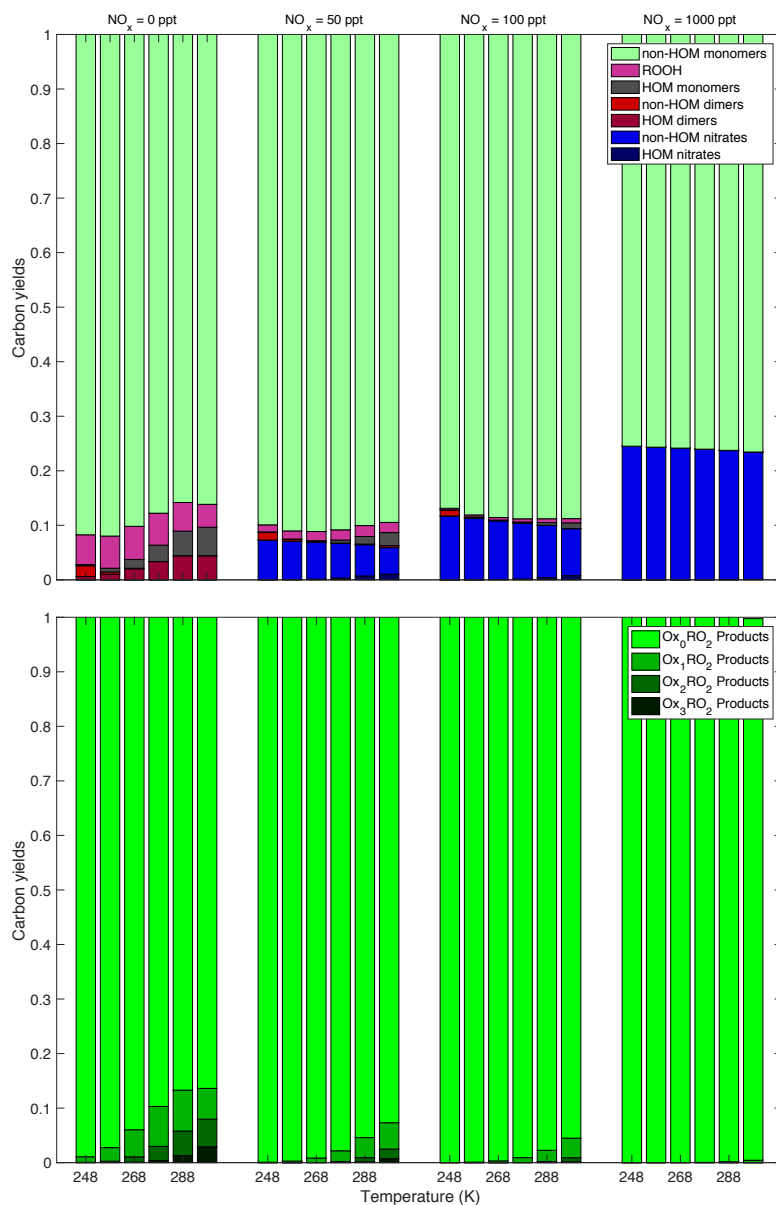


Figure 10. This plot shows the synergistic effect of the NO_x and temperature on the product yields. The same trend persists at every NO_x concentration specifically the decrease in the amount of HOMs—both monomers and dimers with decreasing temperature. Of note is that at the highest NO_x concentration shown here (1000 ppt NO added), the HOM production is close to 0 at every temperature. Thus complete suppression of HOMs occurs around this NO_x concentration. This plot shows both the temperature dependence and the NO_x dependence again, but colors are based on how oxidized the peroxy radical that produced the products were. The products represented by the darker colors underwent more auto-oxidation before terminating than those represented by the lighter colors. We can see that auto-oxidation is suppressed both by temperature and by NO_x . Once again, we see that at a high enough NO_x concentration, auto-oxidation is effectively suppressed at all the temperatures investigated here.